THE "THERMOST" FOR ANALYSING THERMO-STRUCTURAL BEHAVIOUR OF LWR FUEL ROD UNDER PCI CONDITIONS

H. NUNO, S. OGAWA, H. KOBAYASHI
Mitsubishi Atomic Power Industries, Inc.,
Kitabukuro, Omiya, Saitama,
Japan

Abstract

As one of the methods for evaluating the fuel rod performances under power ramping or load following operations, the combined "FROST" and "THERMOST" system has been developed and being brought into practical use. The former had already been presented at Blackpool Meeting in 1978, and the latter is going to be presented in this paper.

The major purpose of the THERMOST is to analyse very detailed thermal and structural fuel behaviours in a rather localized part of fuel rod whereas the FROST deals with whole-rod-wide general performances.

The code handles 2-dimensional thermal and structural analyses simultaneously by using finite element method, in axial section wide or in lateral section wide. It consists of a fundamental FEM system of generalized constitution and its surrounding subroutine system which characterizes fuel behaviours such as temperature distribution, thermal expansion, elastoplasticity, creep, cracking, swelling, growth etc. Thermal analysis is handled by heat conduction and heat transfer elements (6 kinds) and structural analysis by axisymmetric ring and lateral plane elements (6 kinds). Boundary problems such as contact, friction and cracking are treated by gap and crack elements.

A sample calculation of PCI performance on a PWR fuel rod under ramping condition is presented with some inpile test data.

1 Introduction

The whole-rod-wide fuel performance analysis code "FROST"[1][2][3] (Fuel Rod Stress Analysis) was developed in 1976 and it has been utilized mainly for PCI performance analyses of PWR fuel rods. In relation to the recent

increasing demand for the more detailed evaluation of PCI problems associated with load following oriented studies such as power ramping tests, the "THERMOST" (Thermo-Structural Analysis System) code was developed. As its name implies the code consists of thermal analysis part and structural analysis part both being treated by 2-dimensional FEM (Finite Element Method). First, the 3-dimensional one was aimed, but after various studies it was concluded that the system would be rather complicating and trouble making at least for practical applications, and we finally decided to take the system with two 2-dimensional analysis capabilities, i.e. lateral plane analysis (R-θ System) and axisymmetric analysis (R-Z System).

Since THERMOST is based on a regular FEM treatment which usually requires very many discretized elements to handle one particular section of a fuel rod, the code is usually applied to the analysis on a rather localized part of the fuel rod where fuel behaviours are significant. Therefore, as the standard way of evaluating overalled PCI performance of a fuel rod the combined FROST and THERMOST system is utilized at present.

The code is constructed with a central FEM block and surrounding material block which provides with various fuel behaviour models (Fig. 3.1). First, proper functioning of the former block was thoroughly checked in various angles, by using commonly available reference codes such as ANSYS, MARC, etc., especially with emphasis on the material and boundary nonlinear capabilities. And the total function and fuel behaviour characteristics were checked with already established codes such as FROST and PAD (standard fuel design code). After that, the verification on the THERMOST or FROST/THERMOST system has steadily been carried out using the irradiation data from various power ramping tests and commercial reactor operational experiences. One of the verification activities done on the PWR fuel rod power ramping test is presented in this paper. On the other hand, in order to handle number of calculations associated with fuel design improvements, postprocessing capability and interface functions with FROST code were strengthened. And now the system combined FROST and THERMOST has been being brought into practical use in area of LWR fuel PCI analyses.

2 Total Analytical System

The THERMOST is constructed with a regular FEM which usually requires many discretized elements to handle the phenomena of contineous distributions, and from the view point of calculational economy the combined FROST and THERMOST system is usually taken as a total system to evaluate an overall performances of a fuel rod. Fig.2.1 shows the schematic of a typical calculational procedure presently used. First, the whole-rod-wide calculation is performed for the entire period of irradiation time, from which the general fuel performances and characteristics of PCI are revealed. Then the specific portions of the rod under interest are further analyzed by THERMOST for the period when loading conditions are significant. From this detailed analysis, coupled with FROST analysis, the overalled fuel PCI performances are evaluated.

Since the THERMOST calculation usually starts at a certain time during the irradiation, the results of FROST at that moment have to be transfered to THERMOST. The major items to be transfered are dimensions, plastic and creep strains, residual stresses etc. as initial values, and internal pressure, fission gas release, axial PCI forces etc. as time history data. The transfer is done under artificially cooled down and unloaded conditions in order to simplify the take over.

The THERMOST has two basic analytical capabilityies, i.e. "Lateral Plane Analysis" and "Axisymmetric Analysis", and they are properly chosen according to the purpose of analysis.

3 Constitution of THERMOST

The general organization of the THERMOST is shown in Fig.3.1. It consists of a central FEM block and a material block. The former block contains fundamental FEM mechanics both thermal and structural, and the latter block contains various relationships which characterize the objective fuel rod, such as material properties and fuel behaviour models. This block also has the central block control section by which access of material block programs to the central block can be controlled. The user made subprograms of various type are also accessible at specified points in the central block. This program organization makes it very convenient to update or improve the behaviour models and to extend the capabilities of the code.

The THERMOST has two basic analysis capabilities, "Lateral Plane Analysis" (R-θ System) and "Axisymmetric Analysis" (R-Z System), as shown in Fig. 3.2. The former is mainly used for analizing the phenomena with axial variation such as hourglassing of pellet, ridging deformation of clad etc. And the latter is for analyzing circumferential variations such as clad stress and strain concentration caused by the local interaction from cracked or relocated fuel pellets.

The calculation is carried out on either of the above two systems. The calculational model is constructed by assembling the appropriate elements that are prepared in the element library. The element library consists of thermal and structural elements for axial and lateral plane systems as shown in Table 3.1. For the further details of these elements refer to Table 3.2. The material properties and behaviour models called from central block are common to both axial and lateral plane systems. And the finite element meshing is common to both thermal and structural analyses. This kind of program organization helps simplify the code constitution itself and also the handling and maintenance of it.

Fig.3.3 shows general flow diagram of THERMOST. After the initial preparation thermal and structural analyses proceed simultaneously by incremental method following the loading (operational) history. Usually the time mesh of temperature calculation is coarser than structural one.

The structural analysis is proceeded as follows. After setting up the loading increments and boundary condition, non-time dependent strain (i.e. instantly responsible strains) analysis is followed, in which matrix operations associated with elastoplastic and boundary nonlinear characteristics are proceeded with sub-increment and iteration methods. After this block is properly converged the time dependent strain analysis is done, in which strain increments of creep, growth etc. are dealt with also by sub-increment and iteration methods. The residual loadings (treated as errors) generated at afore mentioned convergence calculations are sifted to the next time step, as one of the new loadings, in order to prevent the accumulation of errors.

The calculated results are stored in a data storage for postprocessing or restart calculation use. Various postpocessing capabilities are provided mainly being plotter programs.

4 Fundamental Mechanics of THERMOST

4.1 Thermal Analysis

The temperature distributions in lateral or axial plane are handled by 2-dimensional FEM with steady state treatment. The equilibrium of steady state heat conduction for an element is,[4]

$$[\hat{k}]\{\hat{T}\} + \{\hat{P}\} = \{0\} \tag{4.1}$$

$$[\hat{k}] = \int_\Omega \nabla^T\{N\}[k]\nabla\{N\}^T d\Omega + \int_\Gamma \{N^*\} h \{N\}^T d\Gamma$$

$$\{\hat{T}\} = (T_1\ T_2 \cdots T_4)^T \qquad \text{for 4-Node Element}$$

$$\{\hat{P}\} = \int_\Omega \{N\} Q\, d\Omega + \int_\Gamma \{N^*\}\bar{q}\, d\Gamma - \int_\Gamma \{N^*\} h T_0\, d\Gamma$$

$\{N\}$: Shape Function on Domain Ω

$\{N^*\}$: Interporation Function on Boundary Γ

$[k]$: 2 x 2 Heat Conduction Matrix

$\nabla \equiv \left(\frac{\partial}{\partial x}\ \frac{\partial}{\partial y}\right)^T$: Gradient Operator

Ω : Domain within the Element

Γ : Boundary of the Element

Q : Internal Heat Generation

$\bar{q}$: Heat Flux at Boundary

h : Heat Transfer Coefficient at Boundary

T_0 : Outside Temperature

In case of 4-node lateral plane element, heat flux $\{q\}$ at point (x, y) is,

$$\{q\} = \begin{Bmatrix} q_x \\ q_y \end{Bmatrix} = [k]\nabla T(x,y)$$

Since $\quad T(x,y) = (N_1 \ldots N_4)\cdot(T_1 \ldots T_4)^T$

$$\{q\} = [k]\begin{bmatrix} \frac{\partial N_1}{\partial x} & \frac{\partial N_2}{\partial x} \cdots \\ \frac{\partial N_1}{\partial y} & \frac{\partial N_2}{\partial y} \cdots \end{bmatrix}\begin{Bmatrix} T_1 \\ \vdots \\ T_4 \end{Bmatrix}$$

$$= [k][B]\{T\} \tag{4.2}$$

where $\quad T_1, \ldots T_4$: Temperature at Nodal Points

$T(x,y)$: Temperature at Point (x,y)

Then $[\hat{\mathbf{B}}]$ in eq. (4.1) becomes as,

$$[\hat{H}] = \int_{\Omega} \begin{bmatrix} \frac{\partial N_1}{\partial x} & \frac{\partial N_4}{\partial y} \\ \vdots & \vdots \\ \frac{\partial N_4}{\partial x} & \frac{\partial N_4}{\partial y} \end{bmatrix} \begin{bmatrix} k_{xx} & k_{xy} \\ k_{yx} & k_{yy} \end{bmatrix} \begin{bmatrix} \frac{\partial N_1}{\partial x} & \cdots & \frac{\partial N_4}{\partial x} \\ \frac{\partial N_1}{\partial y} & \cdots & \frac{\partial N_4}{\partial y} \end{bmatrix} d\Omega$$

$$= \int_{\Omega} [B]^T [k] [B] \, d\Omega \qquad (4.3)$$

The equation of heat conduction equilibrium for a gloval system is obtained by combining the element-wise relationship given by eq. (4.1).

$$[H]\{T\} + \{F\} = \{0\} \qquad (4.4)$$

$$\{H\} = \sum^{n} [\hat{H}], \quad \{T\} = \sum^{n} \{\hat{T}\} \quad \text{and} \quad \{F\} = \sum^{n} \{\hat{F}\}$$

4.2 Structural Analysis

The treatment on structural analysis is based on the general structural FEM commonly seen in many literatures such as Ref. [4]~[8], and only fundamental relationships will be described.

4.2.1 Strains Considered in Structural Analysis

$$\{d\varepsilon\} = \{d\varepsilon^e\} + \{d\varepsilon^p\} + \{d\varepsilon^c\} + \{d\varepsilon^T\} + \{d\varepsilon^s\} + \{d\varepsilon^g\} + \{d\varepsilon^H\} + \cdots \qquad (4.5)$$

$\{d\varepsilon\} \equiv (d\varepsilon_x \; d\varepsilon_y \; d\varepsilon_z \; d\gamma_{xy})^T$: Total Strain Increment for Lateral Plane Elements

or $\equiv (d\varepsilon_r \; d\varepsilon_\theta \; d\varepsilon_z \; d\gamma_{r\theta})^T$: Total Strain Increment for Axisymmetric Ring Elements

$\{d\varepsilon^e\}$: Elastic Strain Increment

$\{d\varepsilon^p\}$: Plastic Strain Increment

$\{d\varepsilon^c\}$: Creep Strain Increment

$\{d\varepsilon^T\}$: Thermal Expansion Strain Increment

$\{d\varepsilon^s\}$: Swelling Strain Increment (Solid Swelling & Gas Swelling by Creep, for Pellet)

$\{d\varepsilon^g\}$: Growth Strain Increment (for Clad)

$\{d\varepsilon^H\}$: Hourglassing Strain Increment; for Lateral Plane Element in Pellet Only

4.2.2 Elastic Analysis

Incremental stress-strain relationship in elastic range is dealt with as,

$$\{d\sigma\} = [D^e(T)]\{d\varepsilon^e\} + \frac{\partial[D^e(T)]}{\partial T}\{\varepsilon^e\}dT \qquad (4.6)$$

$\{d\sigma\} = (d\sigma_x\ d\sigma_y\ d\sigma_z\ d\tau_{xy})^T$ for Lateral Plane Elements

$= (d\sigma_r\ d\sigma_\theta\ d\sigma_z\ d\tau_{rz})^T$ for Axisymmetric Elements

$[D^e]$: Elastic Flexibility Matrix

4.2.3 Elastoplastic Analysis for Cladding

Non-volumetric change in plastic deformation ($\sum d\varepsilon_{ii}^p = 0$) and Prager's hardening theory[9] are taken. Yield function is as,

$$f(\{\sigma\},\{\alpha\},T) = f(\{S\}) - K(T) = 0 \qquad (4.7)$$

$\{S\} = (S_x\ S_y\ S_z\ S_{xy})^T = \{\sigma\} - \{\alpha\}$

$\{\sigma\} = (\sigma_x\ \sigma_y\ \sigma_z\ \tau_{xy})^T$

$\{\alpha\} = (\alpha_x\ \alpha_y\ \alpha_z\ \alpha_{xy})^T$: Origin Shift Stress

$K(T)$: Material Yield Stress

$$\{d\alpha\} = C\{d\varepsilon^p\} \qquad (4.8)$$

$C = \frac{2}{3}H_K$

$H_K = \frac{\partial K(T)}{\partial \bar{\varepsilon}_p}$: Strain Hardening Coeff. in Uniaxial Test

As yield criterion, von Mises relation is taken.

$$f = \bar{\sigma} = \sqrt{\frac{3}{2(F+G+H)}}\left[F(S_y-S_z)^2 + G(S_z-S_x)^2 + H(S_x-S_y)^2 + 2NS_{xy}^2\right]^{\frac{1}{2}} \qquad (4.9)$$

F,G,H,N : Anisotropic Parameters

And flow rule is,

$$\{d\varepsilon^p\} = d\lambda\left\{\frac{\partial f}{\partial \sigma}\right\} \qquad (4.10)$$

where $\{\partial f/\partial\sigma\}$ is calculated as,

$$\left\{\frac{\partial f}{\partial \sigma}\right\} = \frac{3}{2\bar{\sigma}}\begin{Bmatrix}\sigma_x'\\ \sigma_y'\\ \sigma_z'\\ 2\tau_{xy}\end{Bmatrix}$$

where

$$\begin{Bmatrix}\sigma_x'\\ \sigma_y'\\ \sigma_z'\\ 2\tau_{xy}\end{Bmatrix} = \frac{1}{F+G+H}\begin{bmatrix}(G+H) & -H & -G & 0\\ -H & (F+H) & -F & 0\\ -G & -F & (F+G) & 0\\ 0 & 0 & 0 & 2N\end{bmatrix}\begin{Bmatrix}S_x\\ S_y\\ S_z\end{Bmatrix} \qquad (4.11)$$

Constitutive equation for the elastoplastic analysis as.

$$\{d\sigma\} = \left[[D^e] - \frac{[D^e]\left\{\frac{\partial f}{\partial \sigma}\right\}\left\{\frac{\partial f}{\partial \sigma}\right\}^T[D^e]}{H_k + \left\{\frac{\partial f}{\partial \sigma}\right\}^T[D^e]\left\{\frac{\partial f}{\partial \sigma}\right\}}\right]\{d\varepsilon^{ep}\}$$

$$+\left[\frac{\partial [D^e]}{\partial T}\{\varepsilon^e\} - \frac{[D^e]\left\{\frac{\partial f}{\partial \sigma}\right\}\left(\left\{\frac{\partial f}{\partial \sigma}\right\}^T \frac{\partial [D^e]}{\partial T}\{\varepsilon^e\} - \frac{\partial K}{\partial T}\right)}{H_k + \left\{\frac{\partial f}{\partial \sigma}\right\}^T[D^e]\left\{\frac{\partial f}{\partial \sigma}\right\}}\right]dT$$

or

$$\equiv [D^{ep}]\{d\varepsilon^{ep}\} + \{\psi^{ep}\}dT \qquad (4.12)$$

$[D^{ep}]$: Elastoplastic Flexibility Matrix

$$\{d\varepsilon^{ep}\} \equiv \{d\varepsilon^e\} + \{d\varepsilon^p\}$$
$$= \{d\varepsilon\} - \{d\varepsilon^c\} - \{d\varepsilon^T\} - \cdots$$

$H_k \equiv C\left\{\frac{\partial f}{\partial \sigma}\right\}^T\left\{\frac{\partial f}{\partial \sigma}\right\} = \frac{3}{2}C$: Inclination of Hardenning

Expressing eq. (4.12) by $\{d\varepsilon\}$ we get final constitutive equation as,

$$\{d\sigma\} = [D^{ep}]\{d\varepsilon\} - [D^{ep}]\{d\varepsilon^c + d\varepsilon^T + \cdots\} + \{\psi^{ep}\}dT$$
$$\equiv [D^{ep}]\{d\varepsilon\} + \{f\} + \{\psi^{ep}\}dT \qquad (4.13)$$

$d\varepsilon^c, d\varepsilon^T, \ldots$ and dT can independently be caluculated by each fuel behaviour calculation according to the previous and present status.

Therefore the 2nd and 3rd terms in the right hand side of eq.(4.13) are known quantities and treated as loadings to the element.

4.2.4 Elastoplastic Analysis for Pellet

For pellet material isotropy is assumed and volumetric change under plastic deformation is considered. The similar relationships to the previous clad material will be described taking up only important portions.

As yield criterion, isotropic hardening and parabolic Mohr-Coulomb Criterion[10] are used.

$$f = (3J_2' + 3\beta J_1'^2)^{\frac{1}{2}} \qquad (4.14)$$

where $J_1' \equiv J_1 + 3P_{pore}$

$J_1 \equiv \sigma_x + \sigma_y + \sigma_z$

$J_2' \equiv \frac{1}{3}\bar{\sigma}^2$

β : Hot Pressing Parameter $= \mathcal{F}(\rho, \sigma_{yield})$, ρ : Density

P_{pore} : Pressure of Gas Inside Pores with Correction by Surface Tension of Pellet Material[14]

The equation corresponding to eq. (4.10) is,

$$\left\{\frac{\partial f}{\partial \sigma}\right\} = \frac{3}{2f}\begin{Bmatrix} \sigma_x' + 2\beta J_1' \\ \sigma_y' + 2\beta J_1' \\ \sigma_z' + 2\beta J_1' \\ 2\tau_{xy} \end{Bmatrix} \tag{4.15}$$

And flow rule is,

$$\{d\varepsilon^p\} = d\lambda\left\{\frac{\partial f}{\partial \sigma}\right\} = \frac{3}{2f} d\lambda\,(\sigma_x' + 2\beta J_1',\ \sigma_y' + 2\beta J_1',\ \sigma_z' + 2\beta J_1',\ 2\tau_{xy})^T \tag{4.16}$$

Here
$$dV = \sum d\varepsilon_{ii}^p = 9\beta J_1' d\lambda \tag{4.17}$$

dV means volumetric change due to the difference between hydrostatic pressure of average normal stress and inside-pore pressure, which directly relates to the hot pressing or the gas pore swelling.

The final constitutive equations for pellet are the same form as eq. (4.12) or eq.(4.13) for clad.

5 Fuel Behaviour Models

The material properties and fuel behaviour models specific to the fuel are handled by the subprograms in the material block (in Fig.3.1). The fuel rod behaviours treated in this code are listed in Table 5.1, and some of them will be explained below.

5.1 Temperature Distribution

As to the temperature analysis the basic relationships described in section 4.1, together with the finite elements in Table 3.2, are applied to both pellet and clad.

If a big void is included in the plane to be analyzed, the special elements with highly softened stiffness and with void-thermal conductivity are defined on that portion, and if a crack is generated in a certain crack element (structural) the heat transfer element is automatically inserted.

Fig.5.1 shows an example of temperature analysis on a lateral plane of a 14x14 type PWR fuel rod, which has been done to reveal the effect of pellet radial cracks to the circumferential temperature distribution.

5.2 Clad Creep

As the standard constitutive equation to account for equivalent creep strain rate, Ibrahim and Ross-Ross type correlation empirically obtained on cold worked zircaloy-4 is used.

$$\bar{\varepsilon}_{th} = f(\bar{\sigma},T)\cdot t^{g(T)} \tag{5.1}$$

$\bar{\varepsilon}_{th}$: Effective Thermal Creep Strain under Constant Loading

$f(\bar{\sigma},T) = A \exp(a+bT+cT\cdot\bar{\sigma})$

$g(T) = d\cdot T + e$

$\bar{\sigma}$: Mises Stress, kg/cm^2

T : Temperature, ^oC

t : Time, sec

A, a, b, c, d, e : Constants

$$\dot{\bar{\varepsilon}}_{irrad} = B\,\bar{\sigma}\,\phi \tag{5.2}$$

$\dot{\bar{\varepsilon}}_{irrad}$: Effective Irradiation Creep Rate, 1/hr

ϕ : Fast Neutron Flux, $n/cm^2/sec$

B : Constant

$$\dot{\bar{\varepsilon}}^c = \dot{\bar{\varepsilon}}_{th} + \dot{\bar{\varepsilon}}_{irrad} \tag{5.3}$$

$\dot{\bar{\varepsilon}}^c$: Total Effective Creep Rate, 1/sec

As to the model to generate instantaneous thermal creep rate (under variable loadings) from eq.(5.1) (which is for constant loadings), presently conventional total strain hardening correlation is used.

$$\dot{\bar{\varepsilon}}_{th} = \frac{g}{\sigma}\cdot f^{\frac{1}{g}}\cdot \bar{\varepsilon}_{th}^{(1-\frac{1}{g})} \tag{5.4}$$

Our recent study on zircaloy-4 cladding creep under variable loading condition revealed that ORNL recommended strain hardening model expressed by strain origin concept[5] well represented the hardening characteristics including under stress reversals, if it was modified with anelastic term attached to it. Presently the revision of the thermal creep model is going to be taken up together with the experiments to clarify the multiaxial problems associated with strong anisotropy and effect of strain history on strain hardening characteristics.

5.3 Pellet Hourglassing Model for Lateral Plane System

Although the hourglassing of a pellet can not be treated rigorously by the lateral plane system, a convenient and practical method of "Hourglass Strain Model" is proposed. The concept of the model is explained in Fig.5.2.

As the preparation, the hypothetical hourglass strain function is established from the parametric calculations done on the basis of elastic and non-cracking condition (for a free standing pellet). In the actual calculation on a lateral plane analysis the incremental hourglass strain is imposed as one of the strain loadings (refer to eq.4.5).

Since the hypothetical strain is imposed, the stress distribution in pellet is more or less different from real one, but so long as the deformation is concerned it is properly estimated by this model. The validity of the model is rechecked, as shown in Fig. 5.3, by comparing the calculational result of this model with corresponding axisymmetric calculation.

The use of this model enables to take into account the hourglassing effect and the circumferential variation effect (e.g. radial cracking) at the same time.

6 A Verification by an Experiment

For the purpose of getting the various informations concerning the failure limits and associated design improvements, the joint project organized by Japanese PWR utilities and Mitsubishi has been being carried out at Studsvik test reactor in Sweden.

The test data aquired from the power ramping tests are also utilized to verify and improve the present analytical system. One of the results of these studies done on the 17 x 17 type PWR test rod will be described below.

6.1 Outline of Ramping Test

The general specification of the test rod, No. "M-2", is shown in Fig. 6.1. The test rod is of a rather standard specification except for intentional lower internal pressurization than standard design in order to enhance PCI intensity at power ramping. The operational history is shwon in Fig. 6.2. After the base irradiation in 3OCA the power ramping test was

carried out in No. 1 loop of R2 reactor. 2-step-wise power ramping was imposed after an appropriate preconditioning time.

The profilometry measurements were made 4 times during base irradiation under cooled down condition and final one at post-irradiation examination, as can be seen in Fig. 6.6. No failure was observed in this rod.

6.2 Analysis System and Calculational Models

The system combined FROST and THERMOST was used for the present calculation. The relationship between FROST and THERMOST in the calculation is explained in Fig. 6.2. First FROST calculation was performed over the entire range of irradiation, thus providing with the necessary input data for the THERMOST calculation that was followed after base irradiation. Transfer of initial values to THERMOST, such as dimensions, was done on the basis of cold and artificially unloaded conditions to simplify the take over.

In the FROST analysis the calculational model was segmented in 3 axial parts and each segment was further divided into 5 rings for pellet and 3 rings for cladding.

In the THERMOST analysis, both R-θ model (Lateral plane) and R-Z model (Axisymmetric) were used. The finite element mesh configurations of them are shown in Fig. 6.3 and 6.4 respectively.

For R-Z model no cracking in pellet was dealt with in this analysis. As to the axial boundary condition the axial forces corresponding to internal and external pressure difference were imposed on cladding and internal gas pressure on pellet, and no rotation was allowed at the top end of cladding. As to the finite element, HRING4 & HCONV4 for thermal analysis, and PLANE4 & GAP2 for structural analysis were used (Refer to Table 3.2). Meshing configuration is always common to both thermal and structural analyses.

For R-θ model 8 radial cracks model was taken. As to the axial boundary loading, the same forces as R-Z model were imposed. To deal with the axial forces the generalized plane strain element with an axial freedom, GPLANE3, was used for the structural analysis, and the other elements used were HPLANE4, HCONV4, GAP2 and CRACK4.

6.3 Comparison of Calculational and Experimental Results

Fig. 6.5 shows the history of the fuel rod internal gas pressure calculated by FROST. The last period of this data, which corresponds to power ramping operation, was used as on of the input to the THERMOST analysis.

Fig. 6.6 shows the history of cladding outside diameter of segment 4 (in Fig.6.2) ciculated by FROST. The corresponding profilometry data are plotted at several points where measurements were made, and very good agreements are observed. Also, the axial profiles before and after the power ramping are shown in Fig. 6.7 comparing the FROST calculations with the measurements, which also show good agreements.

The history of cladding outside diameter during the power ramping cycle is shown in Fig. 6.8 with profilometry plots before and after ramping. Since profilometry measurements were made in 4 different angles to get accurate average diameter, the measured data are presented with a range, say a reliability band, as seen in this figure and also in Fig. 6.9. Fairly good agreement is observed between calculation and experiment. In this figure the sudden bends on the curve at points A' and B' represent initiation and termination of pellet-clad hard-contact respectively, so difference in diameter between A' and B' indicates a permanent deformation which is also shown by the difference between A and B.

Fig. 6.9 shows the axial deformations of clad, i.e. ridge shape, formed by the previous ramping cycle, which correspond to the shape at "B" in Fig. 6.8. The calculations were done by R-Z system and R-θ system independently and the results are shown with profilometry measurements. As to the results of R-Z analysis the ridging hight is a little underestimated comparing with the measurements. This would have been caused by no consideration of radial cracking in pellet for R-Z analysis. R-θ analysis was performed quite separately from R-Z analysis by using "hourglass strain model" described in section 5.3, and also by considering pellet radial cracks (8 crak model). In this case the height of ridge (outside diameter of clad) is properly enhanced as compared with the previous case due to the consideration of pellet cracking. In any case predictions lie almost within the experimental band.

Finally results of stress analysis on clad corresponding to the previous deformation analysis will be shown for reference, although there is no comparable measurement. Fig. 6.10 shows the history of stess in the mid-point of clad at highest ridging position which was analyzed by R-Z system of THERMOST. This corresponds to the deformation analysis in Fig. 6.8. And Fig. 6.11 shows the lateral-plane-wide general deformation pattern and stress distribution of clad in the mid-wall. From these results it could be said that the general trends in the predictions are reasonable and the amounts of them are also considered to be not so deviated from real values. In the above analysis the maximum clad stress during the power ramping is predicted as $\sim$50 kg/cm^2 (depending on μ), while the clad yield stress under the present temperature and irradiation conditions is found as 51 Kg/cm^2 according to MATPRO[15] for instance. Actually failure was not found with this rod. The predicted stress is rather near the level where SCC becomes enhancing. The development of clad failure model including chemical effect like SCC has been being undertaken, and unfortunately it is not available for the present study.

7 Conclusion

(1) For the purpose of detailed PCI analyses in failure evaluation of LWR fuel rods, "THERMOST" code was developed in addition to the existing code "FROST" which deals with a whole-rod-wide fuel bahaviour analyses.

(2) As the standard method of fuel rod performance analysis, the system combined FROST and THERMOST is utilized. First, the FROST calculates general performances over an entire fuel rod for the total irradiation period. Then it is followed by the THERMOST calculation done on the specific fuel rod sections of interest for the period of significant loading conditions.

(3) The THERMOST consists of thermal and structural analysis parts both being created by the regular FEM of two kinds of 2-dimensional analyses i.e. "Lateral Plane (R-θ) System" and "Axisymmetric (R-Z) System". The finite element meshing system is common to both thermal and structural analyses and also both calculations are proceeded simultaneously, thus making the both analyses quite consistent.

(4) The axisymmetric system is mainly utilized for the predictions of PCI characteristics in an axial section like ridge formation due to hourglassing or chamfer effect etc., and lateral plane system is for the predictions of circumferential variations like clad stress/strain concentrations (thinning) or cracking due to localized interaction from pellets.

(5) The THERMOST has been being verified with various irradiation data on LWR fuel rods. One of the verification calculations done on a PWR fuel rod power ramping test carried out in Sweden is presented, in which good agreements in clad deformations between predictions and measurements are found.

(6) The code verifying efforts will steadily be continued on the irradiation tests including power ramping tests currently being undertaken, in order to increase the reliability and also to extend the analytical capabilities such as clad failure mechanism with chemical effect. And the THERMOST together with the FROST is expected to serve as a reliable fuel failure evaluation system in the area of LWR fuels.

8 References

[1] H.Nuno et al, "FROST Code for Predicting Fuel Rod Performance", IAEA Specialists' Meeting, Blackpool, U.K., March, 1978

[2] H.Nuno et al, "The FROST Code for Analizing In-Reactor Behaviours of LWR Fuel Rod", Enlarged Halden Programme Meeting, Loen, Norway June, 1978

[3] H.Nuno et al, "FROST Code for Predicting In-Reactor Behaviours of LWR Fuel Rod", 4th SMIRT, D1/4, 1979

[4] O.C. Zienkiewiz, "The Finit Element Method", 3rd ed., 1977 McGrow-Hill

[5] C.E.Pugh, J.M.Corum, K.C.Liu and W.L.Greenstreet, "Currently Recommended Constitutive Equations for Inelastic Design Analysis of FFTF Components", ORNL-TM-3602, 1972

[6] Y.R.Rashid, "On Nonlinear Kinematic Hardening Plasticity Theory" Nuclear Engineering and Design, Vol.29, 1974

[7] S.Banerjee, R.J.Bridges, J.J.M.Too, "A Model for Analysis of Fuel Behaviour in Transient", Nuclear Engineering and Design, Vol.42, 1977

[8] M.Ichikawa et al, "FEMAXI, An Axisymmetric Finite Element Programme of The Project for Analysis of Local Fuel Rod Deformation", IFA Halden Reactor Project,PC-Note 1632 Octo. 1975

[9] R.Hill, "The Mathematical Theory of Plasticity", The Oxford Engineering Science Series, 1960, Oxford Univ. Press

[10] Y.R.Rashid et al, "Mathematical Treatment of Hot Pressing of Reactor Fuel", Nuclear Engineering and Design, Vol.29 (1974)

[11] M.S.Seltzer et al, "A Review of Creep Behaviour of Ceramic Nuclear Fuels", Reactor Technology, Vol.14, No.2, 1971

[12] H.Nuno et al, "On The Treatment of Numerical Problems Due to Rapid Creep Rate in The Fuel Performance Calculation by FEM", IAEA pecialists' Meeting, Blackpool, U.K., March, 1980

[13] M.L.Lyons et al, "Analysis of UO_2 Grain Growth Data from Out of Pile Experiments", GEAP-4411, Nov., 1963

[14] E.Duncombe et al, "CYGRO-3 A Computor Program to Determine Temperature, Stresses and Deformations in Oxide Fuel Rods", WAPD-TM-961, 1970

[15] D.L.Hagrman, G.A.Reymann,"MATPRO VERSION 11 A Handbook of Materials Properties for Use in The Analysis of Light Water Reactor Fuel Rod Behaviour", NUREG/CR-0497, TREE-1280, 1979

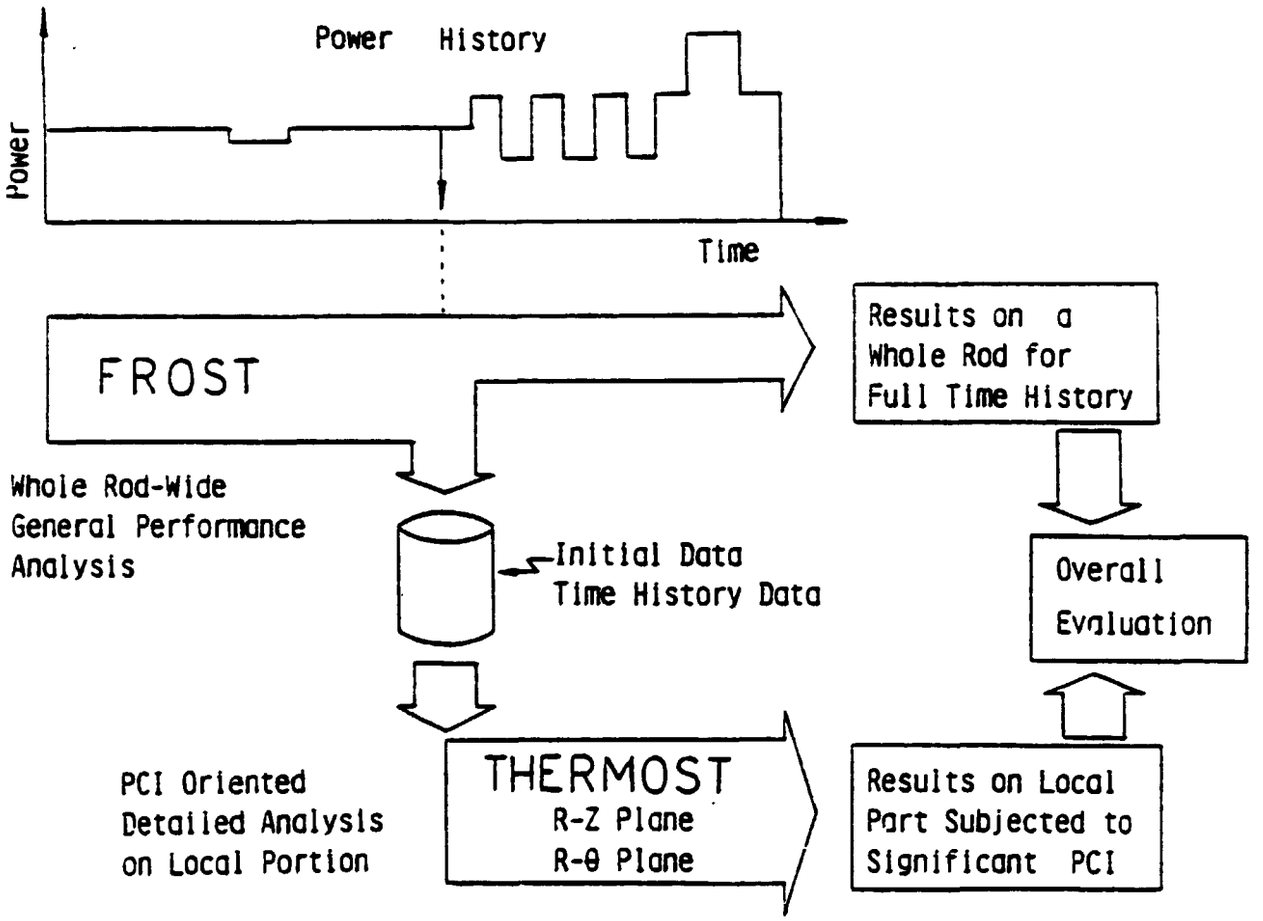

Fig. 2.1 Total Fuel Performance Analysis System

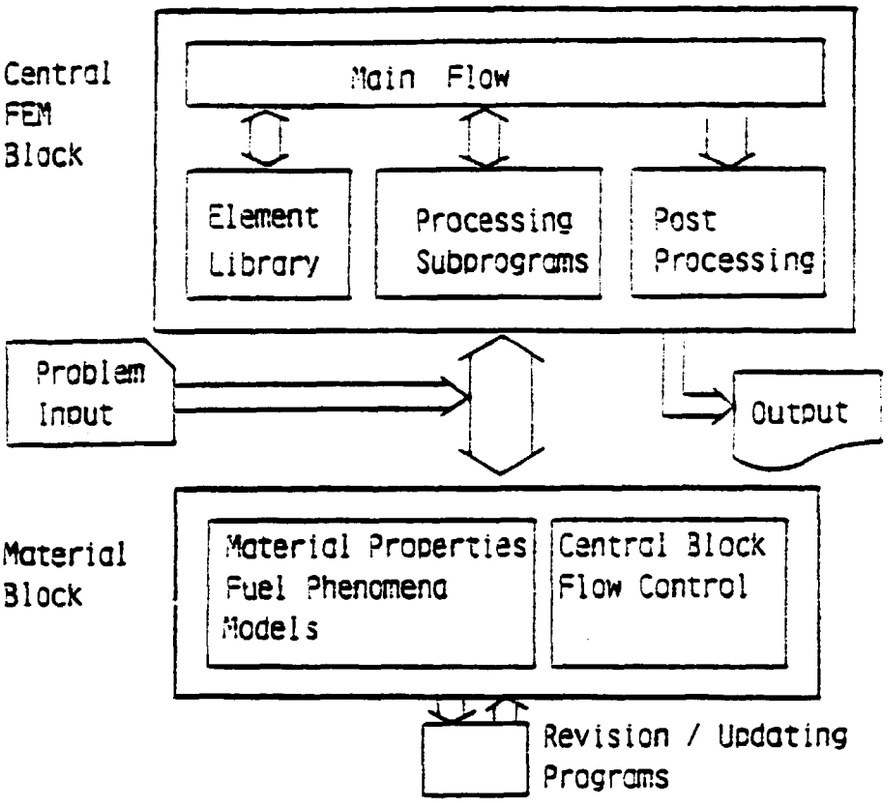

Fig. 3.1 THERMOST Program Organization

Table 3.1 THERMOST Analysis System & Element Library

	Axisymmetric Analysis	Lateral Plane Analysis
Thermal Analysis	Axisymmetric Ring Heat Conduction Element	2-Dimensional Heat Conduction Element
	Heat Transfer Element	
Structural Analysis	Asisymmetric Ring Element	2-Dimensional Plane Element
	Gap/Crack Element	

Table 3.2 List of Library Elements

Category		Name of Element	Explanation n:Node, G:Integral Point, P:Pressure Loading
Thermal Analysis	Lateral Elements	HPLANE4	4-Node Isoparametric Heat Conduction Element 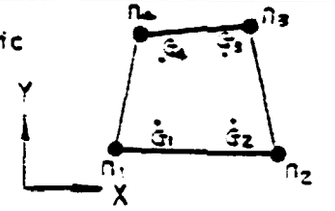
		HPLANE8	8-Node Isoparametric Heat Conduction Element 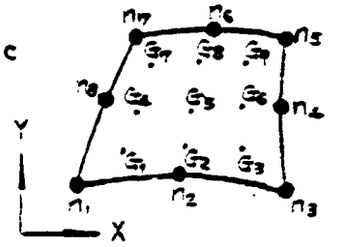
	Lateral & Axisymmetric	HCONV4	4-Node Heat Transfer Element 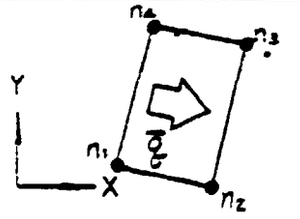
	Axisymmetric Elements	HRING4	4-Node Isoparametric Heat Conduction Ring Element 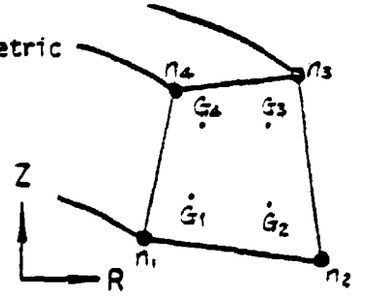
Structural Analysis	Lateral Section Elements	PLANE4	4-Node Isoparametric Plane Stress/Strain Element Plane Stress or Strain by Input Key Anisotropy of E, ν Considered 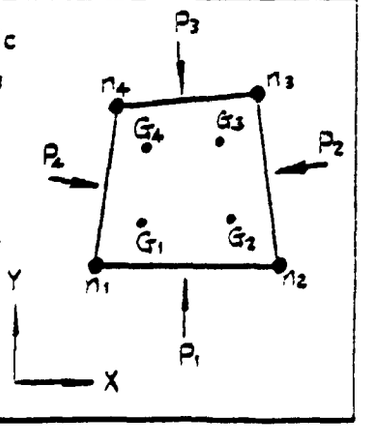

Table 3.2 (Continued)

Structural Analysis	Lateral Section Elements	PLANE8	8-Node Isoparametric Plane Stress/Strain Element. Same as PLANE4 Except for Number of n & G
		GPLANE5	5-Node Isoparametric Generalized Plane Strain Element Arbitrary Constraints on Strain Normal to the Plane can be Imposed on n_5 Anisotropy Considered 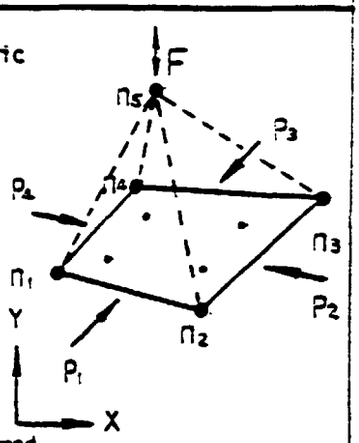
		GPLANE9	9-Node Isoparametric Generalized Plane Strain Element Same as GPLANE5 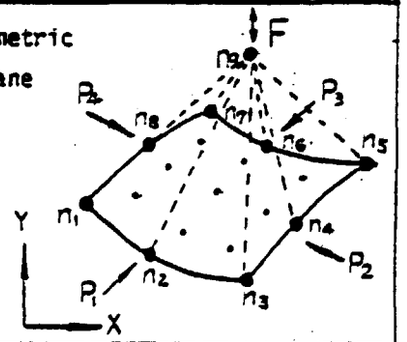
	Axial Section Elements	QAX4	4-Node Isoparametric Ring Element Anisotropy Considered 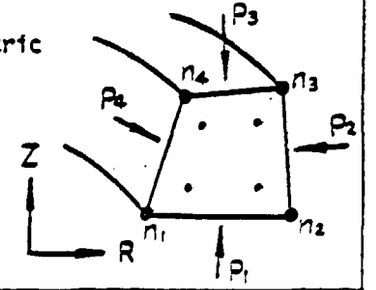
		QAX8	8-Node Isoparametric Ring Element Anisotropy Considered 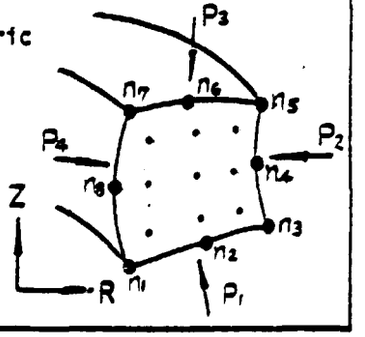

Table 3.2 (Continued)

Structural Boundary Elements	Gap Element	GAP2	2-Node Single Spring Element Between 2 Nodes 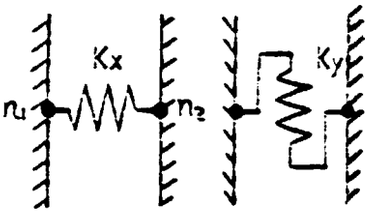 Open/Close Handled by Softening/Stiffening Kx Friction/Slippage by Stiffening/Softening Ky
	Crack Element	CRACK4	4-Node Multi-Spring Element Between Element Junction 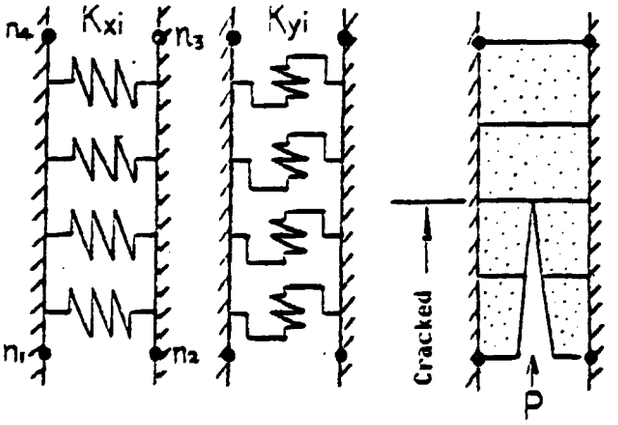 Crack Initiation & Gradual Propergation Handled by Multi-Spring Layout Nonlinear Stress-Strain Relation on Kxi & Kyi Handled Open/Close Handled Same as GAP2 Pressure/Atomosphere Penetration Considered

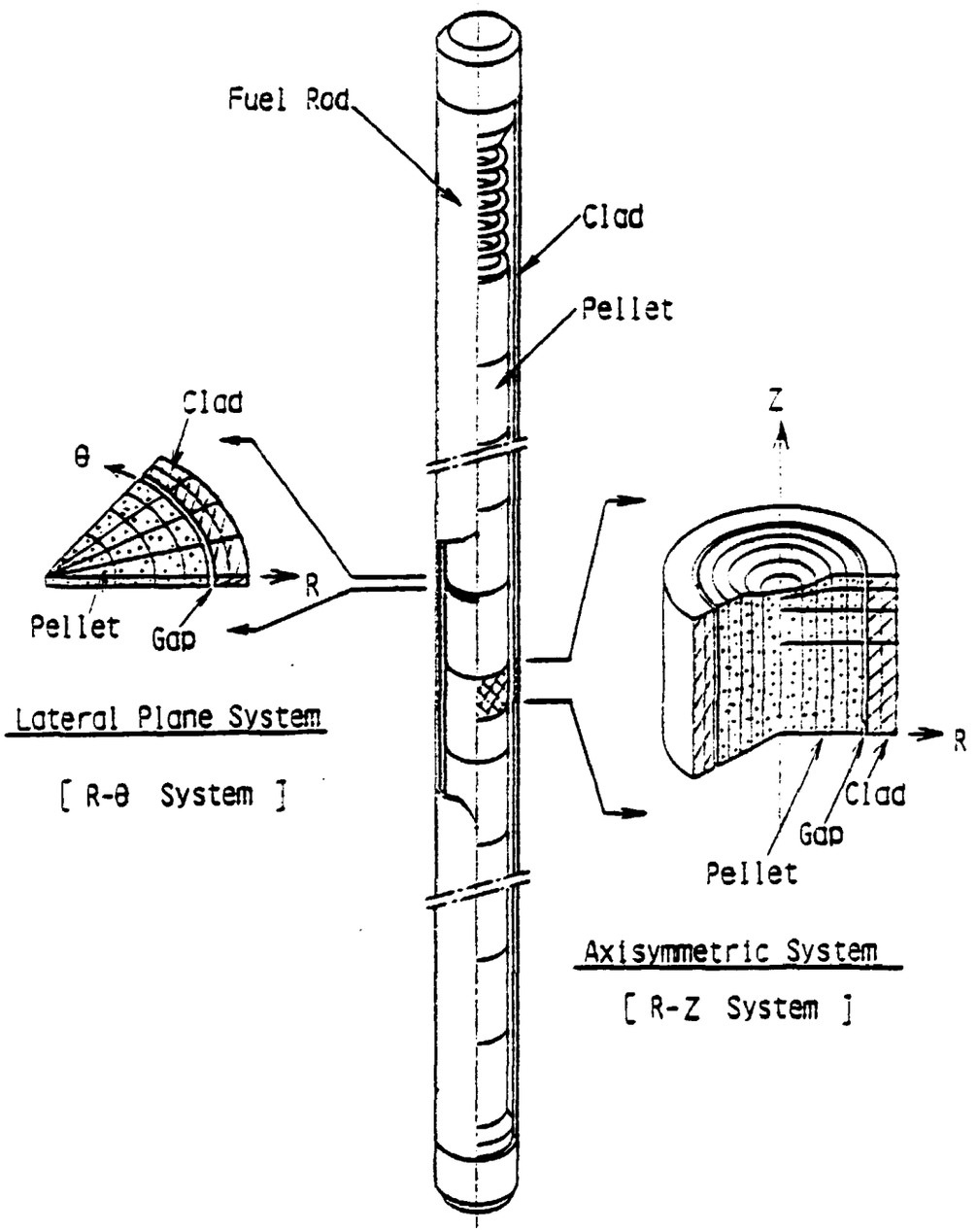

Fig. 3.2 Axisymmetric & Lateral Plane Analysis System in THERMOST

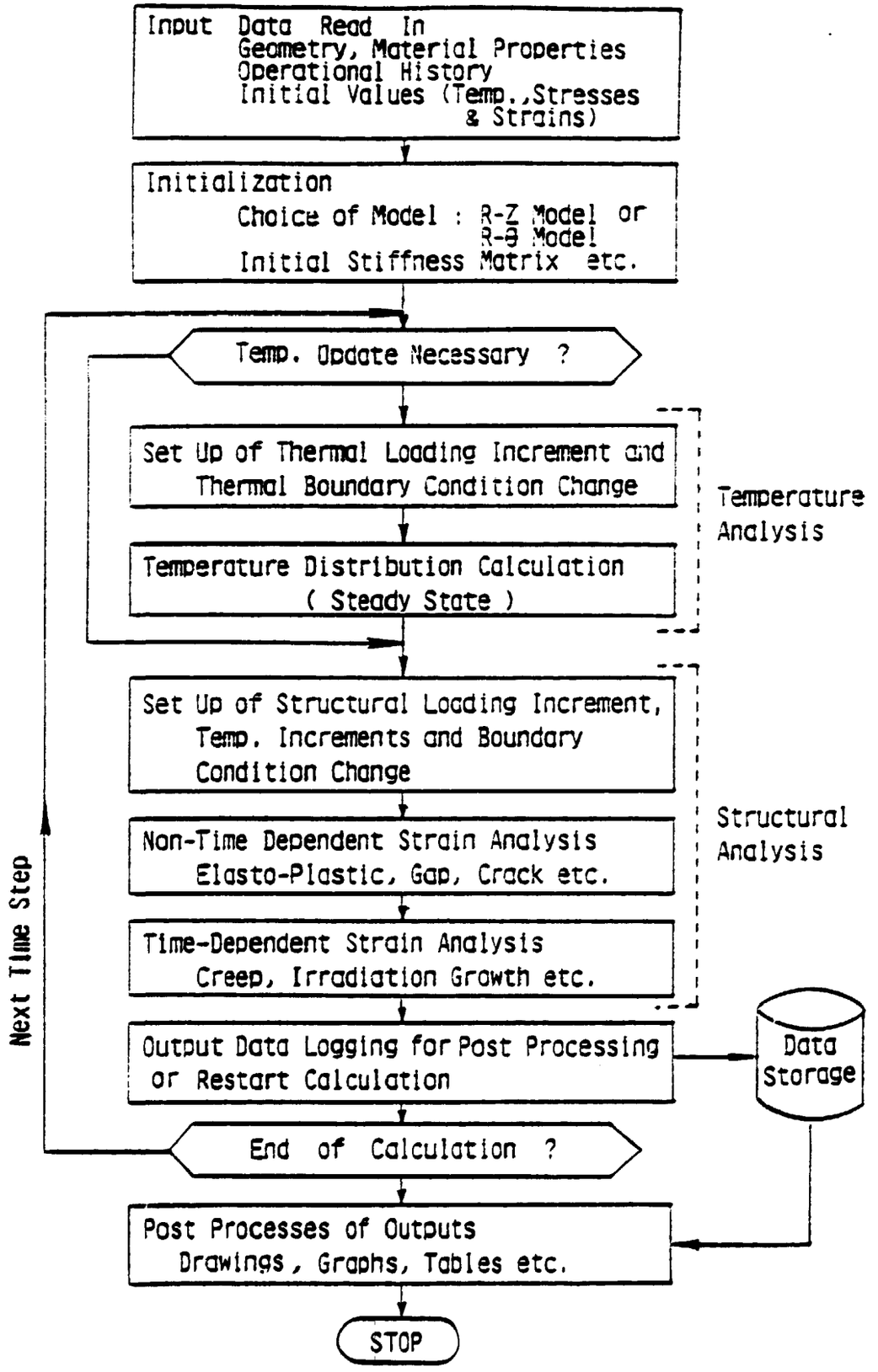

Fig. 3.3 Flow Chart of THERMOST

Table 5.1 Fuel Phenomena Treated in THERMOST

CATEG.	ITEMS	EXPLANATION
CLADDING	Temperature Distribution	Thermal Conductivity $k_{xx}(T)$, $k_{yy}(T)$ for Lateral Plane Elements $k_{rr}(T)$, $k_{zz}(T)$ for Axisymmetric Elements
	Thermal Expansion	Thermal Expansion Coefficient $\alpha_{xx}(T)$, $\alpha_{yy}(T)$, $\alpha_{zz}(T)$
	Elastic	Elastic Properties $E_{xx}(T)$, $E_{yy}(T)$, $E_{zz}(T)$ $\nu_{xy}(T)$, $\nu_{yz}(T)$, $\nu_{zx}(T)$
	Elastoplastic	Dealt by Elastoplastic Matrix $[D^{ep}]$, with Anisotropy Considered. Details in Section 4.2.3
	Creep	Empirical Correlation $\dot{\bar{\varepsilon}}_{th} = f(\bar{\sigma}, T, \bar{\varepsilon}_H, \dot{\phi})$, etc. Details in Section 5.2
	Growth	Anisotropic Growth $\{\varepsilon\}_g = \begin{Bmatrix} A_r \\ A_\theta \\ A_z \end{Bmatrix} f(\phi)$ ϕ: Fast Neutron Fluence
	Crack	Dealt by Crack Element (CRACK4) in Table 3.2

Table 5.1 (Continued)

CATEG.	ITEMS	EXPLANATION
PELLET	Temperature Distribution	Isotropic Thermal Conductivity $k_{xx} = k_{yy} = k_{zz} = k(T,P)$ P : Porosity Heat Transfer through Crack Interface $H_{crack} = K_{mix}/(a+\delta) + bT_K^3$ K_{mix}: Mixed Gas Conductivity δ : Crack Width T_K : Absolute Temp. a,b : Constants Effect of Big Void on Temp. is Treated by Conductivity of Void k_v (usually $= K_{mix}$) k_{ii} , H_{crack} and k_v are Transfered to Thermal Analysis Elements
	Thermal Expansion	Isotropic Thermal Expansion $\alpha_{xx} = \alpha_{yy} = \alpha_{zz} = \alpha(T)$
	Elastic	Isotropic Elastic Properties $E_{xx} = E_{yy} = E_{zz} = E(T,P)$ $\nu_{xy} = \nu_{yx} = \nu_{zx} = \nu(T,P)$ Transfered to Stractural Elements
	Elastoplastic	Dealt by Elastoplastic Matrix $[D^{ep}]$, with Isotropic Assumption and with Hot Pressing Considered. Details in Section 4.2

Table 5.1 (Continued)

CATEG.	ITEMS	EXPLANATION
PELLET	Creep	Seltzer Type Correlation with Isotropic Treatment [11], [12] $\dot{\bar{\varepsilon}} = f(\bar{\sigma}, T, \dot{F}, D)$ $\dot{F}$: Fission Rate D : Grain Size Hot Pressing by Creep ; Optional use
	Grain Growth	Calculated Based on Lyons Model [13] $D = [D_0^3 + \alpha t \exp(-Q/RT)]^{\frac{1}{3}}$ and Used for Creep Calculation
	Swelling	Solid : Empirical Correlation Gas Pore : Dealt by Hot Pressing
	FP Gas Release	Solid : Empirical Correlation Gas Pore : Dealt by Hot Pressing Correlation and by Creep
	Cracking	By (1) Discrete Crack Element (CRACK4) or (2) Homogeneous Stiffness Softening Method [14] Mainly Used to Account for Radial Crack Effect in Axi-symmetric Analysis
	Hot Pressing	Dealt with in Elastoplastic and Creep Analysis.
	Hourglassing	For Axisymmetric Analysis, Automatically Considered For Lateral Plane Analysis "Hourglass Strain Model" is Applied Details in Section 5.3

Table 5.1 (Continued)

CATEG.	ITEMS	EXPLANATION
PELLET	Relocation	Empirical Model , Mostly Dealt with in FROST Analysis at Present
FUEL ROD	Gap Conductance	Thermal Conductance Between Pellet and Clad $H_{gap} = f(K_{mix}(T), \delta, \zeta, P)$ K_{mix}: Mixed Gas Conductivity δ : Gap Width ζ : Surface Rughness of Pellet P : Contact Pressure
	Film Conductance	Thermal Conductance Between Clad and Coolant $H_{film} = f(h_f, K_c, \delta)$ Below Nucleate Boiling $= f(q, T_s, T_c, T_w)$ Under Nucleate Boiling h_f : Film Heat Transfer Coeff. K_c : Heat Conductivity of Clad δ : Thickness of Clad q : Heat Flux T_s : Saturation Temperature T_c : Clad Surface Temperature T_w : Bulk Coolant Temperature
	Internal Gas Pressure	Presently Inputted from "FROST" as Time History
	FP Gas Release	Same as Above , Used for Temperature Calculation

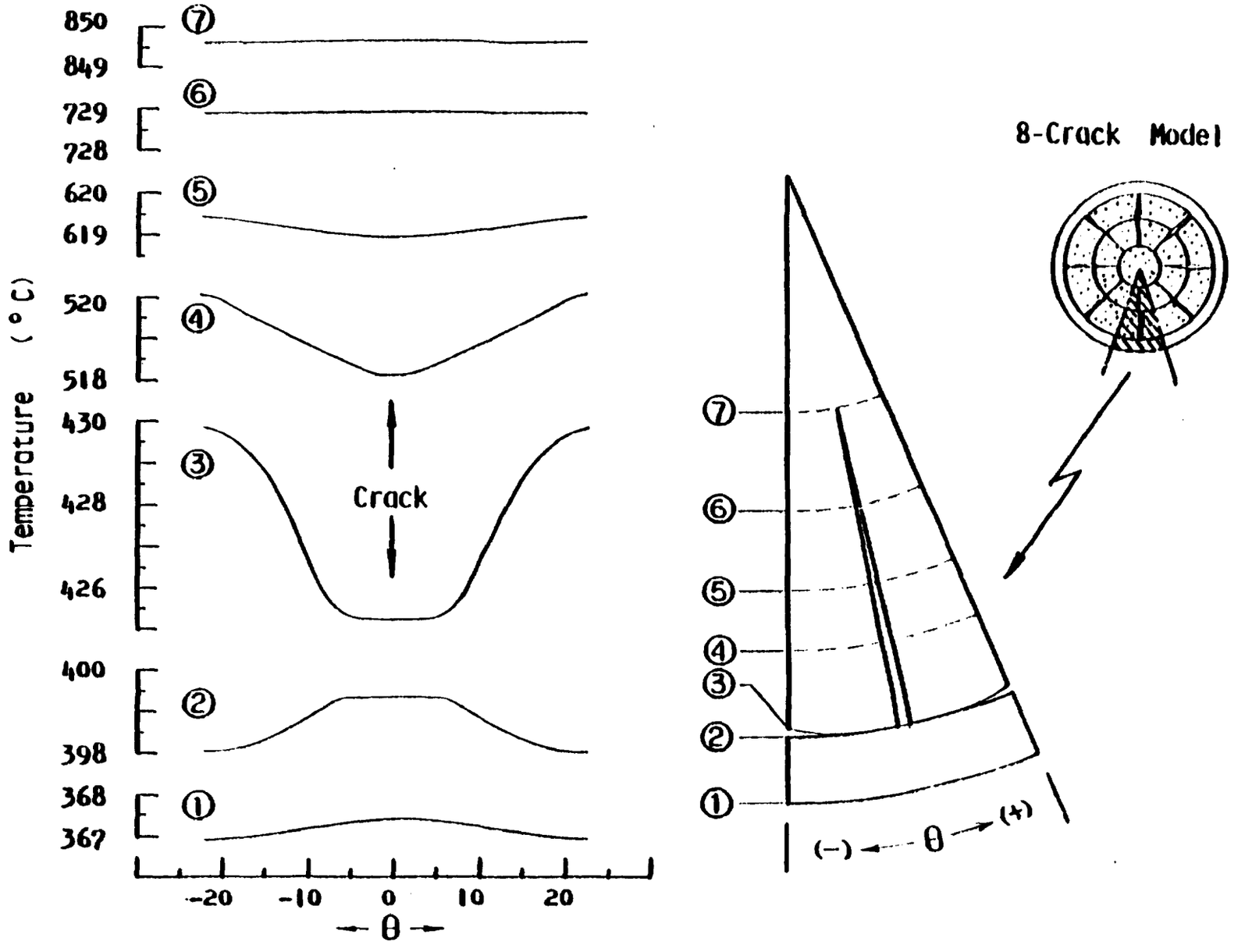

Fig. 5.1 An Example of Temperature Calculation in a Lateral Plane of a 14x14 Type PHR Fuel Rod, with 26 Kw/m of LHR

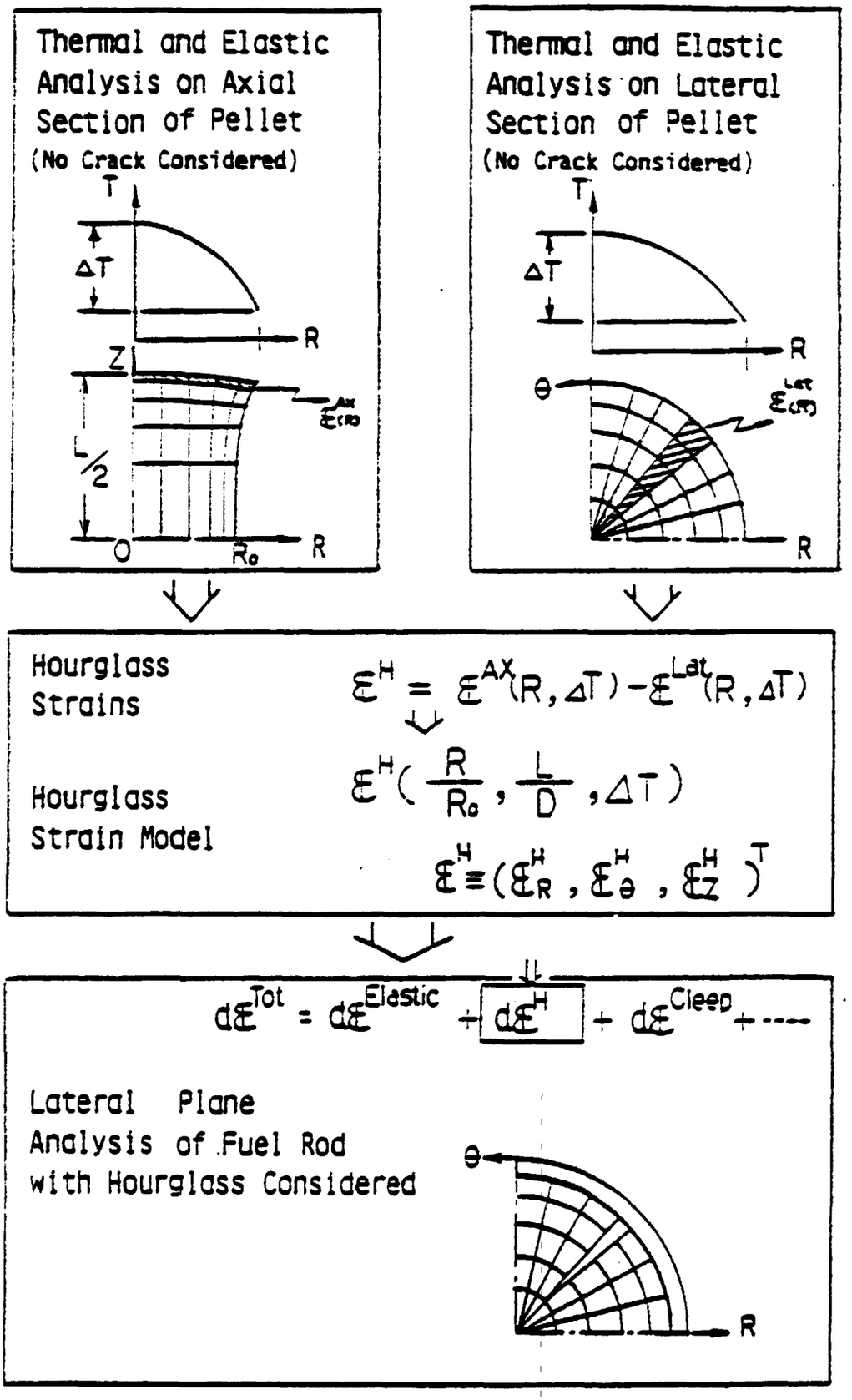

Fig. 5.2 Hourglass Strain Model Applied to Lateral Plane (R-θ System) Analysis

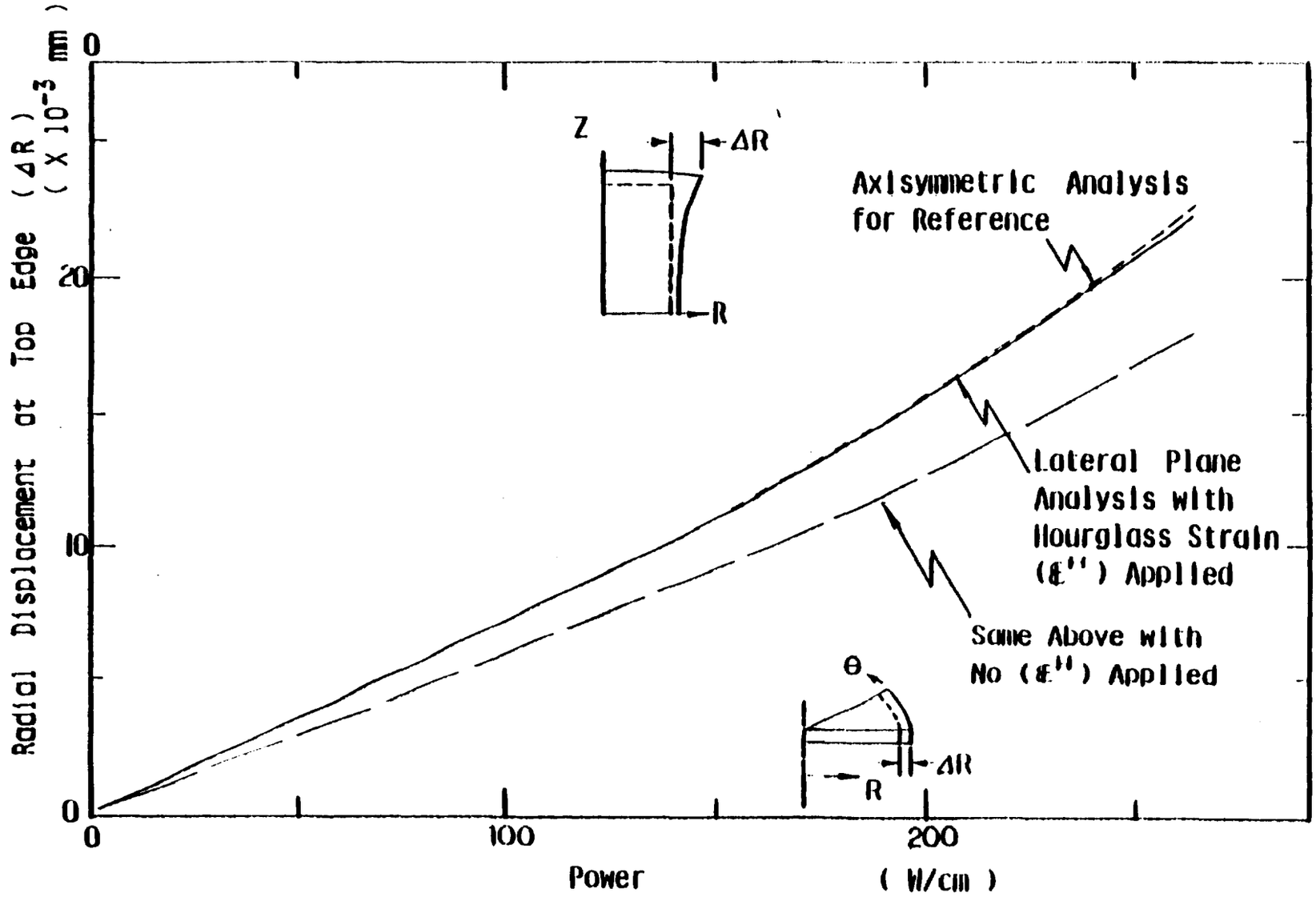

Fig. 5.3

Calculational Verification of Hourglass Model (17x17 Type Fuel Rod)

FUEL ROD TYPE		17X17 PWR ROD
FUEL CLADDING		
	MATERIAL	ZIRCALOY - 4
	O.D.	9.50 mm
	WALL THICKNESS	0.57 mm
FUEL PELLET		
	MATERIAL	UO_2 SINTERED
	O.D.	8.19 mm
	LENGTH	13.5 mm
	SHAPE	DISHED BOTH ENDS
	DENSITY	95 % T.D.
	ENRICHMENT	3.20 W/O
FUEL ROD		
	FILLED GAS	14 Kg/cm^2g He
	DIAMETRAL GAP	0.17 mm

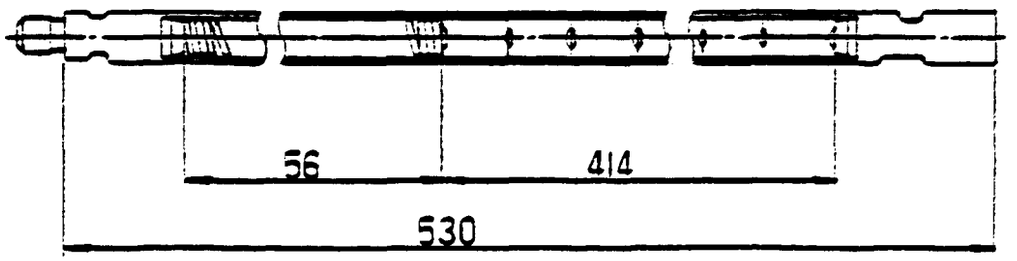

Fig. 6.1 General Specification of Test Rod (#M2)

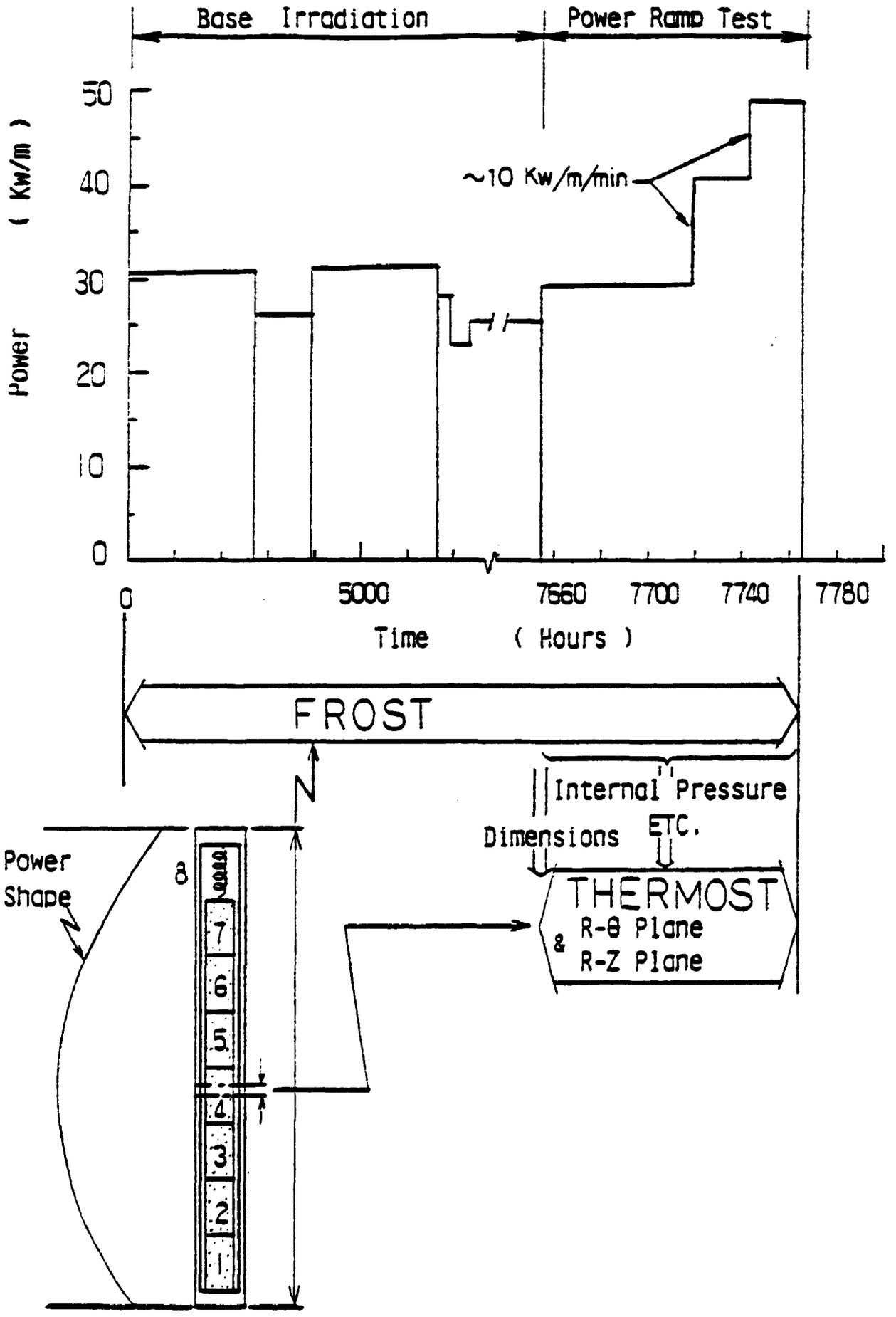

Fig. 6.2 Operational Condition Analysis System

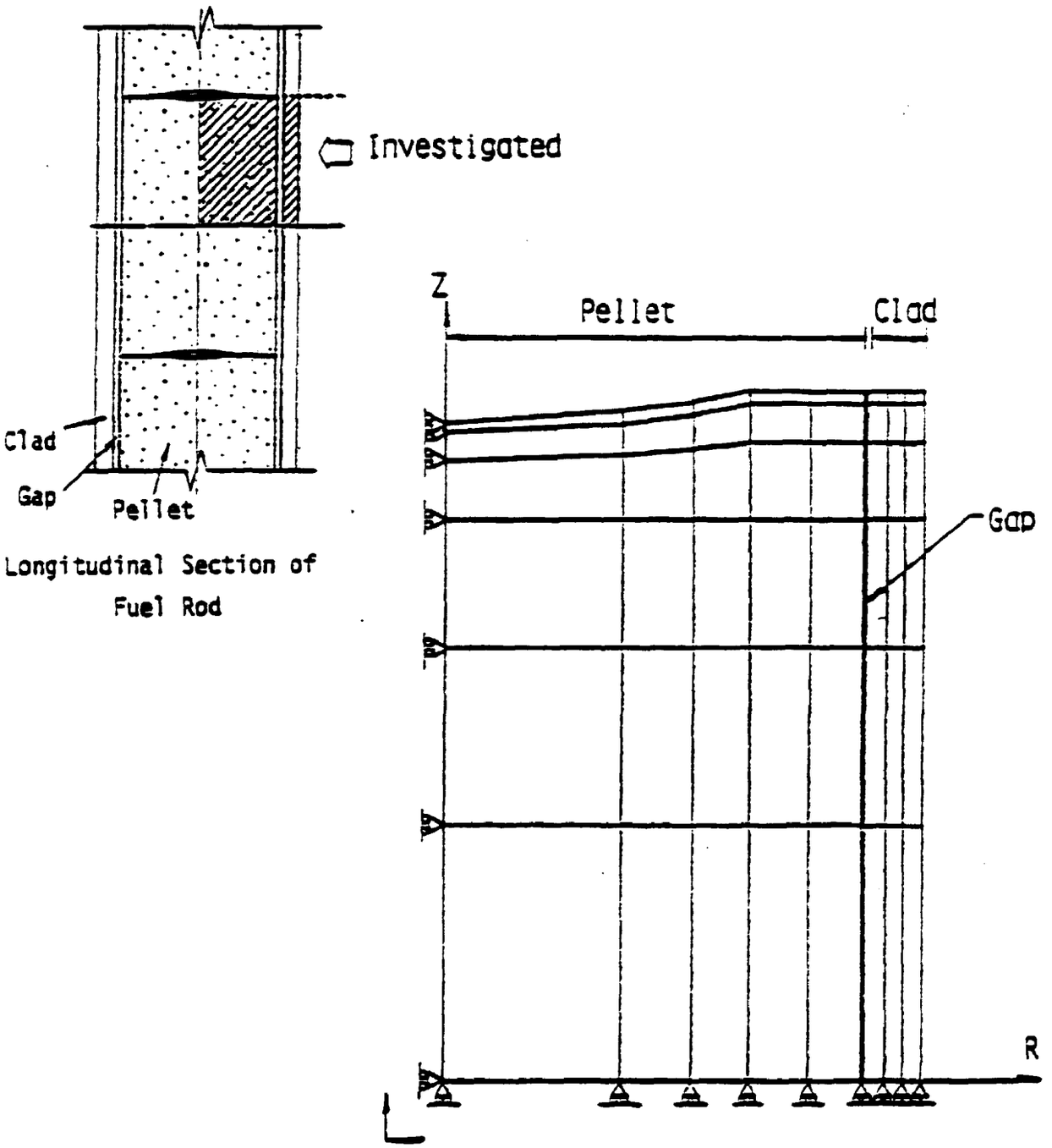

Fig. 6.3 Axisymmetric Model of THERMOST

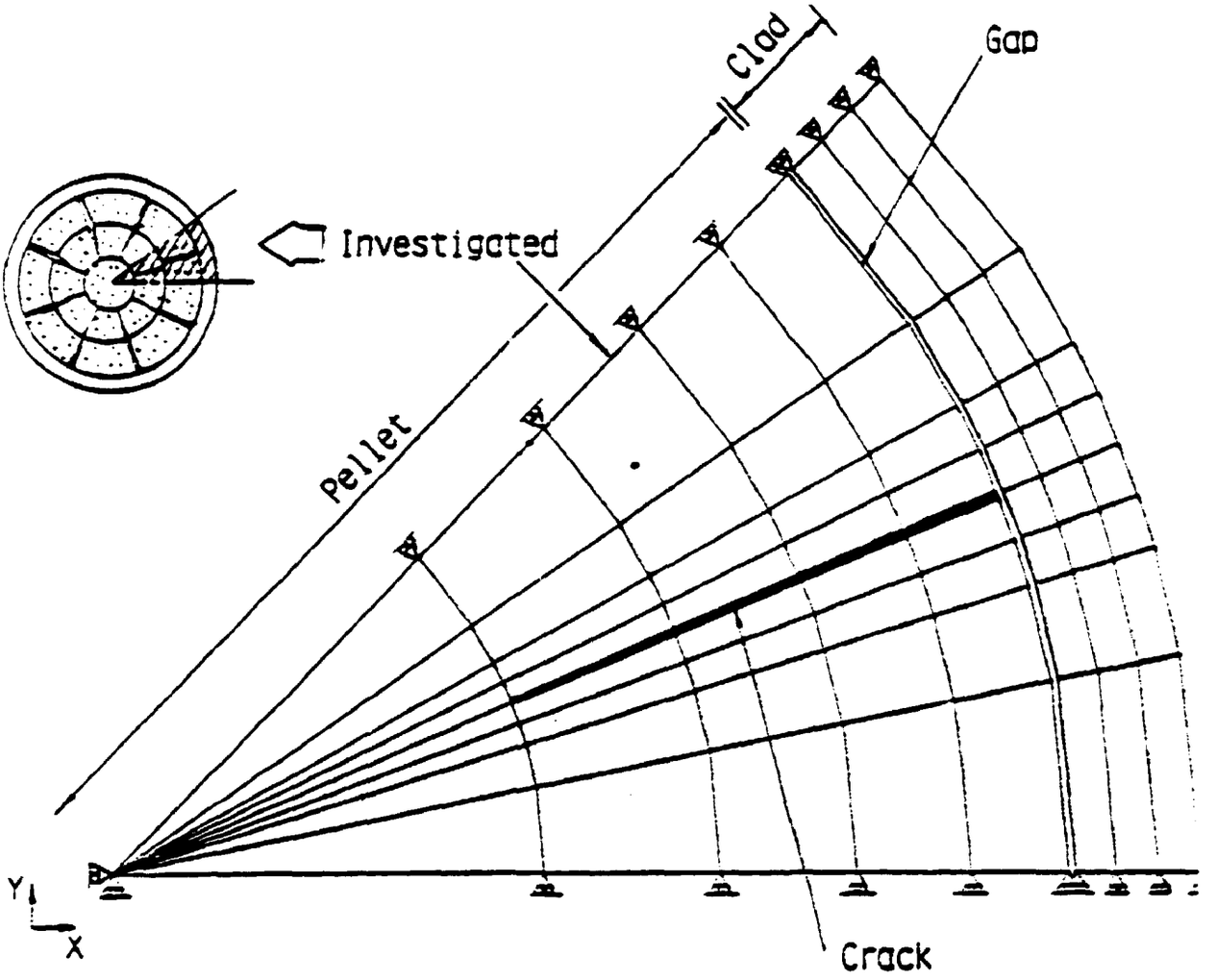

Fig. 6.4 Lateral Plane Model of THERMOST (8-Crack Model

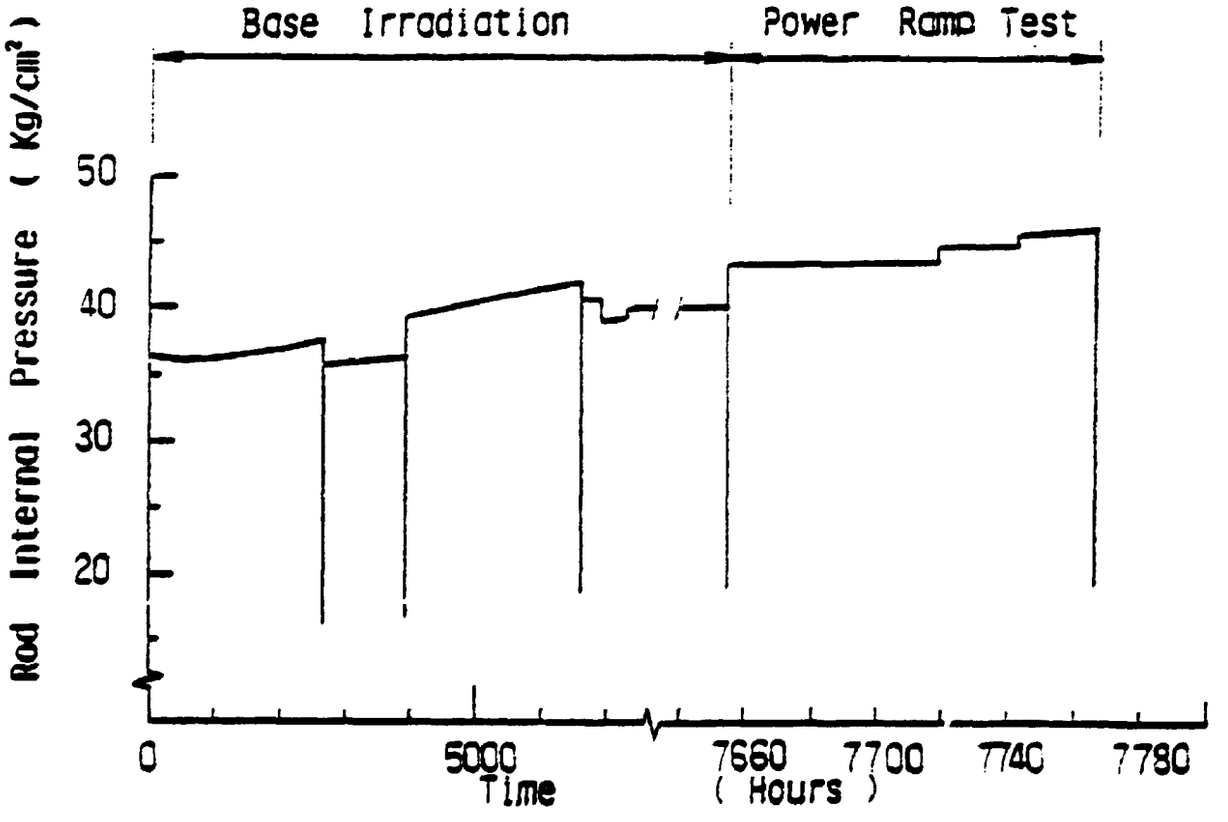

Fig. 6.5 Fuel Rod Internal Gas Pressure (by FROST)

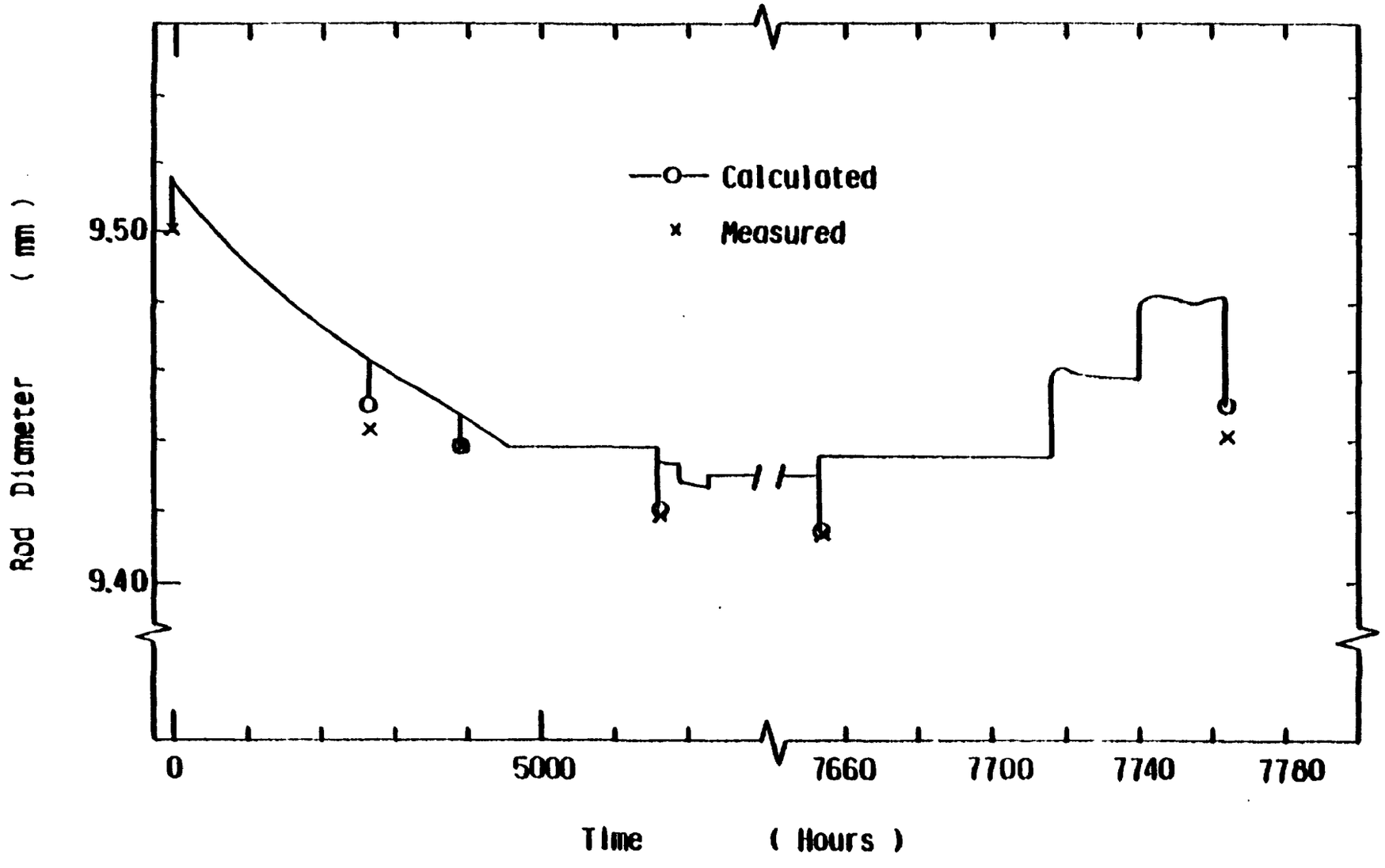

Fig. 6.6 History of Fuel Rod Outside Diameter (by FROST , Segment 4)

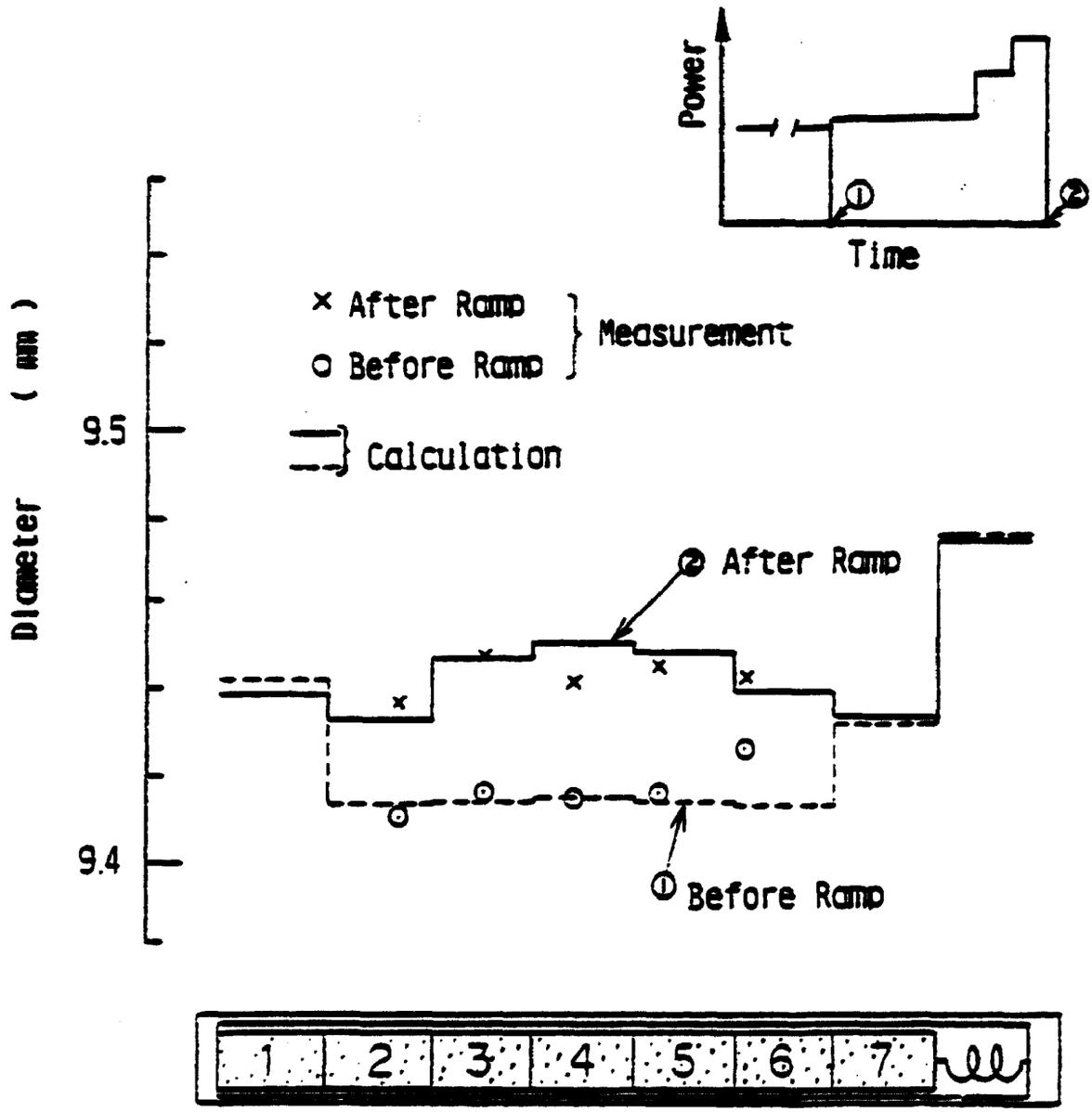

Fig. 6.7 Diametral Profiles Before and After Power Ramping (by FROST)

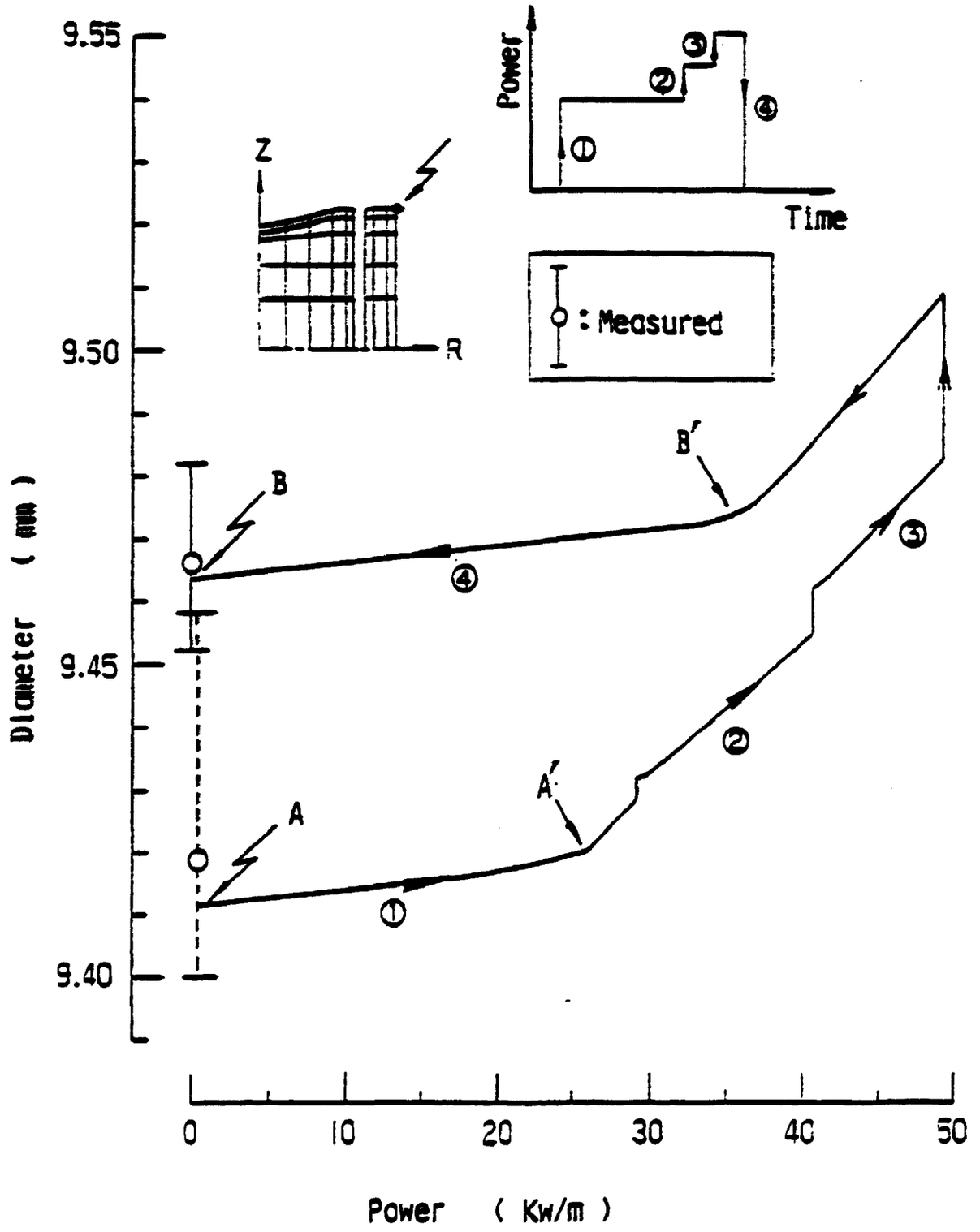

Fig. 6.8 Linear Heat Rate vs. Diameter

(by THERMOST R-Z System)

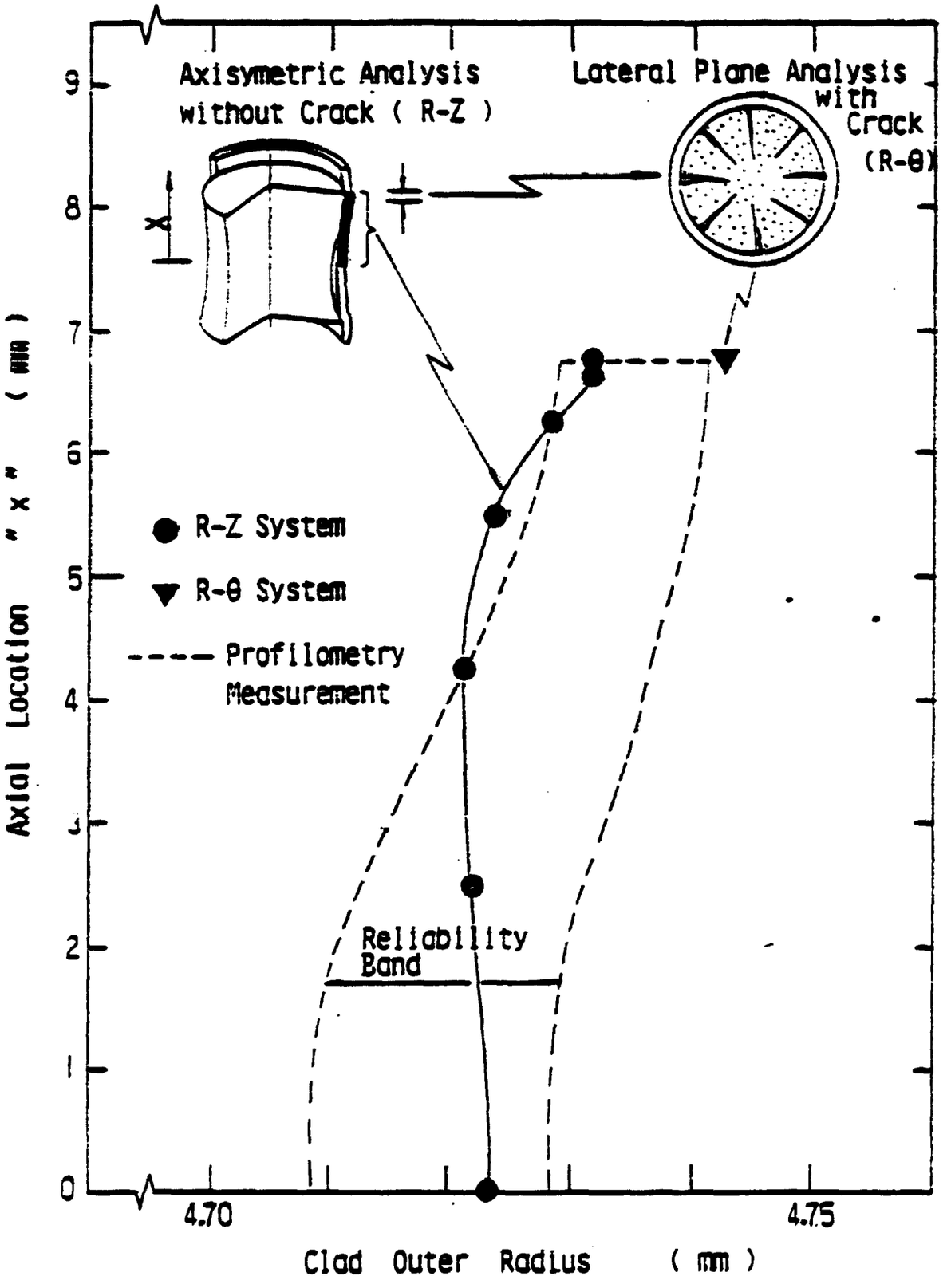

Fig. 6.9 Comparison of Ridge Shapes After Power Ramping

(by THERMOST R-Z and R-θ Systems)

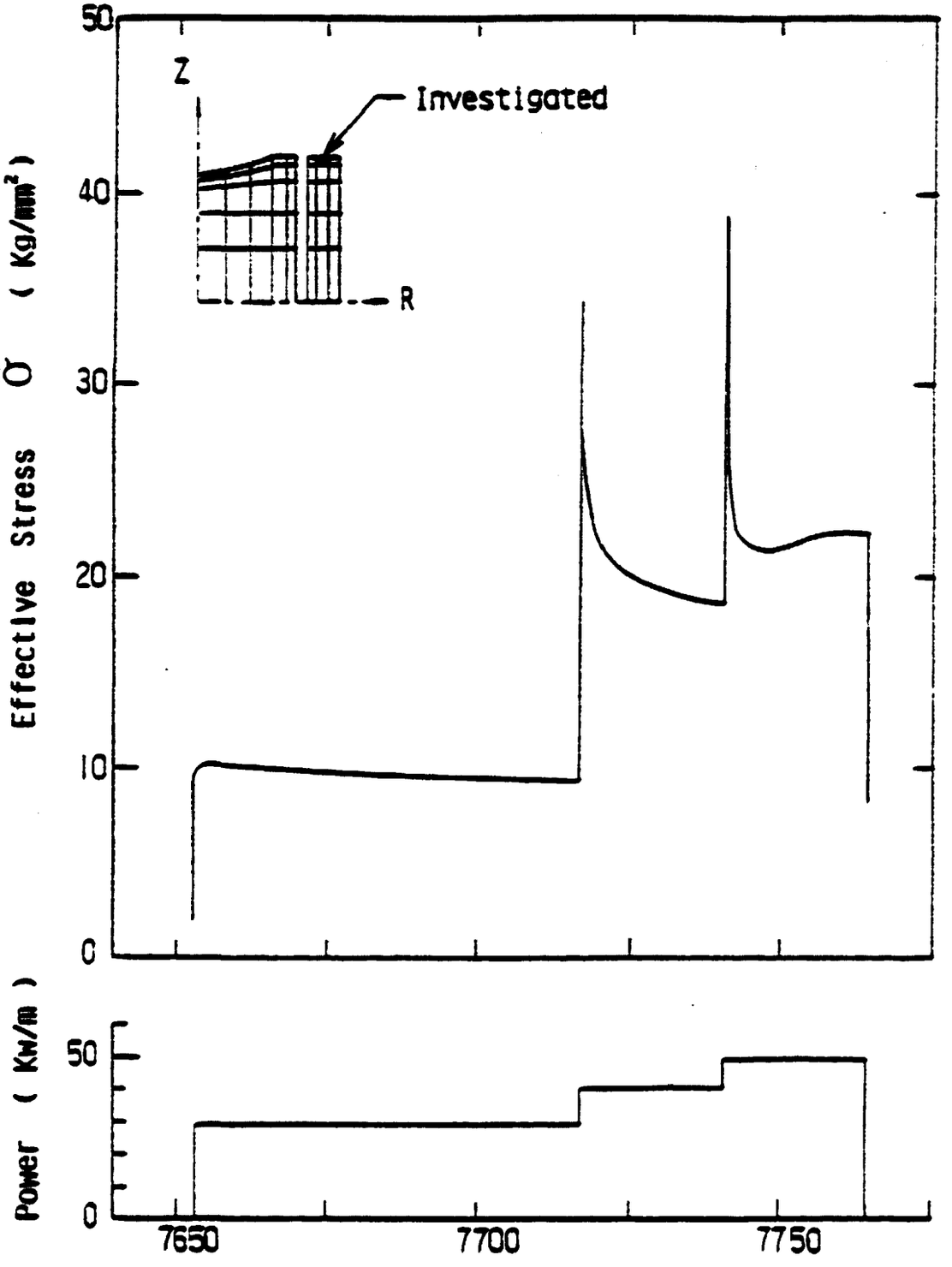

Fig. 6.10 History of Stress in Clad During Power Ramping (by THERMOST R-Z System)

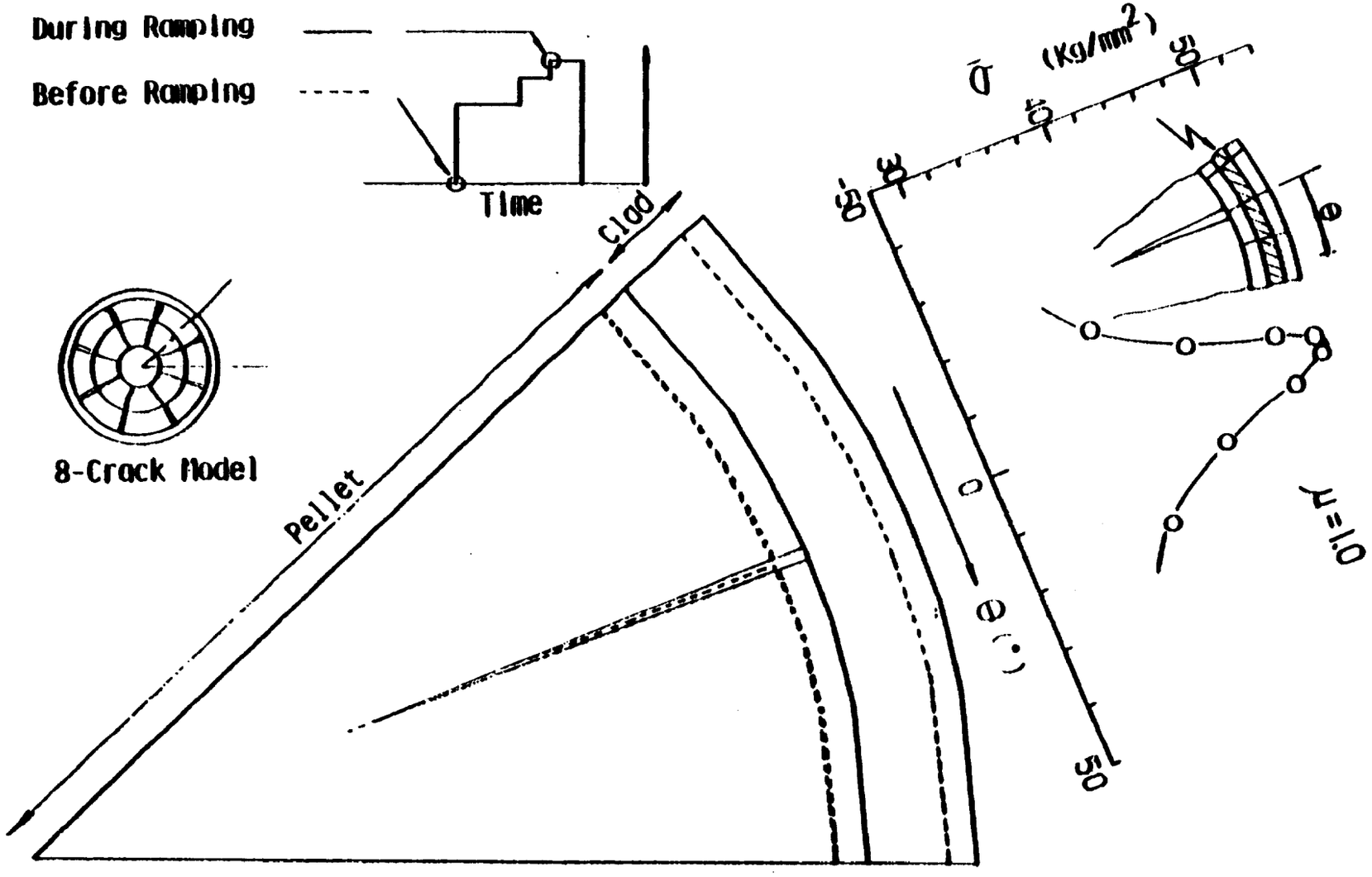

Fig. 6.11 Stress Concentration and Deformation of Clad Arround Pellet Crack Opening (by THERMOST R-0 System)